Geomorphology xxx (2016) xxx–xxx

Contents lists available at ScienceDirect

Geomorphology

journal homepage: www.elsevier.com/locate/geomorph

A watershed scale spatially-distributed model for streambank erosion rate driven by channel curvature

Mitchell McMillan*, Zhiyong Hu

The University of West Florida, Department of Earth and Environmental Sciences, Pensacola, FL, United States

ARTICLE INFO

Article history:
Received 11 November 2016
Received in revised form 20 March 2017
Accepted 21 March 2017
Available online xxxx

Keywords:
Geographic information systems
Root distribution
Meandering streams
Hydraulic modeling

ABSTRACT

Streambank erosion is a major source of fluvial sediment, but few large-scale, spatially distributed models exist to quantify streambank erosion rates. We introduce a spatially distributed model for streambank erosion applicable to sinuous, single-thread channels. We argue that such a model can adequately characterize streambank erosion rates, measured at the outsides of bends over a 2-year time period, throughout a large region. The model is based on the widely-used excess-velocity equation and comprised three components: a physics-based hydrodynamic model, a large-scale 1-dimensional model of average monthly discharge, and an empirical bank erodibility parameterization. The hydrodynamic submodel requires inputs of channel centerline, slope, width, depth, friction factor, and a scour factor *A*; the large-scale watershed submodel utilizes watershed-averaged monthly outputs of the Noah-2.8 land surface model; bank erodibility is based on tree cover and bank height as proxies for root density. The model was calibrated with erosion rates measured in sand-bed streams throughout the northern Gulf of Mexico coastal plain. The calibrated model outperforms a purely empirical model, as well as a model based only on excess velocity, illustrating the utility of combining a physics-based hydrodynamic model with an empirical bank erodibility relationship. The model could be improved by incorporating spatial variability in channel roughness and the hydrodynamic scour factor, which are here assumed constant. A reach-scale application of the model is illustrated on ~1 km of a medium-sized, mixed forest-pasture stream, where the model identifies streambank erosion hotspots on forested and non-forested bends.

1. Introduction

Streambank erosion is one of the most visible ways that rivers adjust to changes in discharge, sediment supply, and floodplain composition (Leopold and Wolman, 1960). Outer bank erosion, along with inner bank accretion, is responsible for meander migration and the long-term evolution of river channel planforms (Crosato, 2009; Parker et al., 2011; Eke et al., 2014). Not only a key physical process, bank erosion creates and maintains diverse riparian habitats, supplies river channels with large woody material (Florsheim et al., 2008), and is a major source of fluvial sediment (Bull, 1997; Sekely et al., 2002; Kronvang et al., 2013). Over the last few decades, it has become clear that accelerated bank erosion is often a signature of human impacts such as channelization (Hupp and Simon, 1991), agriculture (Knox, 2006; Walter and Merritts, 2008; Kemp et al., 2016), and the pervasive construction and demise of milldams (Pizzuto and O'Neal, 2009; Merritts et al., 2011; Lyons et al., 2015). In the U.S., streambank erosion is a major nonpoint source of sediment pollution (U.S. Environmental Protection Agency, 2000). As fluvial systems adjust to increasing human influences (Gregory, 2006), it is important to understand how rates of streambank erosion may respond to changes in land use/land cover, runoff, and other climate variables (Pelletier et al., 2015).

Previous studies have investigated the processes that control rates of bank erosion, including weathering, fluvial erosion, and mass wasting. In sinuous channels, flow around meander bends results in the development of a helical secondary flow, directed inward near the channel bed (Leopold and Wolman, 1960), that produces characteristic bed geometry patterns of shallow point bars and deep pools (Hooke, 1975). The modified bed geometry shifts the primary flow toward the deeper portions of the channel and the outer banks of meander bends (Hooke, 1975; Dietrich et al., 1979; Dietrich and Smith, 1983). These two processes increase the shear stresses acting on the bank, which leads to basal scour and bank steepening. With continued steepening, geotechnical instability and eventually bank failure occur (Thorne, 1982; Lawler et al., 1997), possibly followed by slump block armoring (Parker et al., 2011). Failure is resisted by

* Corresponding author.
E-mail addresses: mcmillan@students.uwf.edu (M. McMillan), zhu@uwf.edu (Z. Hu).

http://dx.doi.org/10.1016/j.geomorph.2017.03.017
0169-555X/

effective cohesion, matric suction, and mechanical reinforcement by vegetation roots (Osman and Thorne, 1988; Simon et al., 2000; Pollen and Simon, 2005; Pollen, 2007; Thomas and Pollen-Bankhead, 2010). Although other bank erosion mechanisms dominate in other channel types, this paper is concerned with modeling bank erosion due to channel curvature.

Although near-bank shear stress is forced by channel curvature variations, the flow does not instantaneously adapt to these variations; a spatial lag develops between maximum curvature and maximum shear stress (Crosato, 2009). The spatial lag distance is proportional flow depth and inversely proportional to channel roughness (Blanckaert and de Vriend, 2010), and can be dramatically decreased by vegetation and vegetation-induced bank irregularities (Thorne and Furbish, 1995), further reinforcing the fundamental importance of bank vegetation in the spatial and temporal evolution of streambanks.

Floodplain heterogeneity, including the spatial arrangement of vegetation patches, soil characteristics, and land cover types, is an important control on the overall patterns of meandering river channels (Güneralp and Rhoads, 2011). Below-ground root distributions remain difficult to quantify, but observations have shown that streambank erosion rates are often sensitive to biomass density (Micheli and Kirchner, 2002; Perucca et al., 2007), root density (Micheli and Kirchner, 2002; Wynn and Mostaghimi, 2006), forest cover (Stott, 1997; Micheli et al., 2004; Allmendinger et al., 2005; Hubble et al., 2010), tree density (Pizzuto and Meckelnburg, 1989; Sass and Keane, 2012; Konsoer et al., 2016), and soil properties such as texture and bulk density (Pizzuto, 1984; Couper, 2003; Julian and Torres, 2006; Wynn and Mostaghimi, 2006; Konsoer et al., 2016). On the other hand, recent work on bank erodibility using jet erosion tests suggests that site-specific (rather than watershed-scale) relationships must be derived from soil properties to estimate bank erodibility parameters (Daly et al., 2015). This suggests that while a purely mechanical model of bank failure is likely to require intensive collection of local data, geospatial data such as tree cover may be used as a proxy for some important aspects of bank erodibility such as root reinforcement.

For cohesive sediments, fluvial erosion is often modeled as proportional to the magnitude of near-bank shear stress above some critical value (Partheniades, 1965). Existing models of streambank erosion have quantified near-bank shear stress in a variety of ways. Following the work of Ikeda et al. (1981), a hierarchy of coupled hydrodynamic-morphodynamic models has been developed based on the assumption that bank erosion rate ζ (m/s) is proportional to the excess near-bank velocity,

$$\zeta = E\Delta U \tag{1}$$

where ΔU (m/s) is the near-bank excess velocity (near-bank velocity u_b minus reach-averaged velocity U_s), and E is a dimensionless calibration coefficient often called the bank erodibility coefficient (Camporeale et al., 2007). Although it is sometimes assumed that the so-called erodibility coefficient depends only on soil and vegetation properties, it also accounts for numerical constants related to the implementation of a given hydrodynamic model (Mosselman, 2014) as well as any processes of opposite-bank accretion that also drive meander migration (Crosato, 2009; Parker et al., 2011). The excess velocity relationship can be thought of as a linearized form of the excess shear stress equation, and has been tentatively confirmed by field observations (Odgaard, 1987; Odgaard, 1989; Pizzuto and Meckelnburg, 1989) and long-term simulations of natural river reaches (Matsubara and Howard, 2014). Eq. (1) is an example of a geomorphic transport law (Dietrich et al., 2003).

Models are already available for quantifying soil erosion and transport from drainage basins, but they lack a bank erosion component (de Vente et al., 2013). The applied community (e.g., stream restoration practitioners) employ field-based, empirical models such as Rosgen's BANCS to estimate bank erosion rates (Rosgen, 2001; Simon and Doyle, 2007; Rosgen, 2009), but researchers attempting to calibrate such models have reported mixed results (Harmel et al., 1999; Van Eps et al., 2004; Sass and Keane, 2012; Kwan and Swanson, 2014; McMillan, 2016). Heavy reliance on visual estimates (e.g., of root density), the need for extensive field data collection, and the lack of a process-based near-bank shear stress model diminish the utility of this approach. A recent attempt to extend the BANCS approach with aerial imagery and GIS data demonstrated the need for a spatially distributed bank erosion model, but itself was limited by its empirical, semi-quantitative approach (Bandyopadhyay et al., 2014). While it is impractical to directly simulate all of the processes responsible for erosion at every streambank, a combination of physics-based modeling with empirical calibration can yield powerful predictive tools (e.g., Pelletier, 2012).

In this paper, we test the hypothesis that a curvature-driven model of bank erosion, parameterized by remotely sensed data, can adequately represent point measurements of bank retreat at the outsides of bends over a large region after calibration by field observations obtained over a 2-year period. The model of this paper quantifies annual streambank erosion rates by employing three interacting submodels: (1) a large-scale, 1-dimensional flow model of monthly discharge and steady uniform flow (streamflow submodel), (2) a physics-based hydrodynamic flow model (hydrodynamic submodel), and (3) a model of bank erodibility based on tree cover and bank height (bank erodibility submodel). These submodels, along with their assumptions and limitations are detailed below. Fig. 1 gives a high-level overview of these components, their data requirements, and how they fit into the conceptual model (transport law) for bank erosion.

2. Model components

Streambank erosion rate $\hat{\zeta}$ (m/year) was modeled as

$$\hat{\zeta} = E\overline{\Delta U} \tag{2}$$

where $\overline{\Delta U}$ (m/s) is the average near-bank velocity excess for a given simulation period, and E is bank erodibility (here with units of s/year). A large-scale 1-dimensional model for streamflow was coupled to a hydrodynamic model to estimate ΔU. Two empirical, spatially distributed bank erodibility parameterizations of E were investigated. For model calibration, simulation periods ranged from 22 to 24 months for each location, depending on the dates of erosion rate measurements. Table 1 summarizes the model input data.

2.1. Monthly streamflow model

Rather than assuming mean annual discharge or bankfull discharge, a large-scale, 1-dimensional model for streamflow was included to account for spatial and temporal variability in runoff. This component was necessitated by the occurrence of sporadic high precipitation events in the study area, which seemed to be correlated to bank erosion events based on our field experience. The goal of the streamflow model is to estimate monthly flow depth H_m and reach-average velocity U for input into the hydrodynamic model. For H_m, Manning's equation can be written in terms of discharge as

$$Q = \frac{1}{n}\frac{A_c^{5/3}}{P^{2/3}}S^{1/2} \tag{3}$$

Please cite this article as: M. McMillan, Z. Hu, A watershed scale spatially-distributed model for streambank erosion rate driven by channel curvature, Geomorphology (2016), http://dx.doi.org/10.1016/j.geomorph.2017.03.017

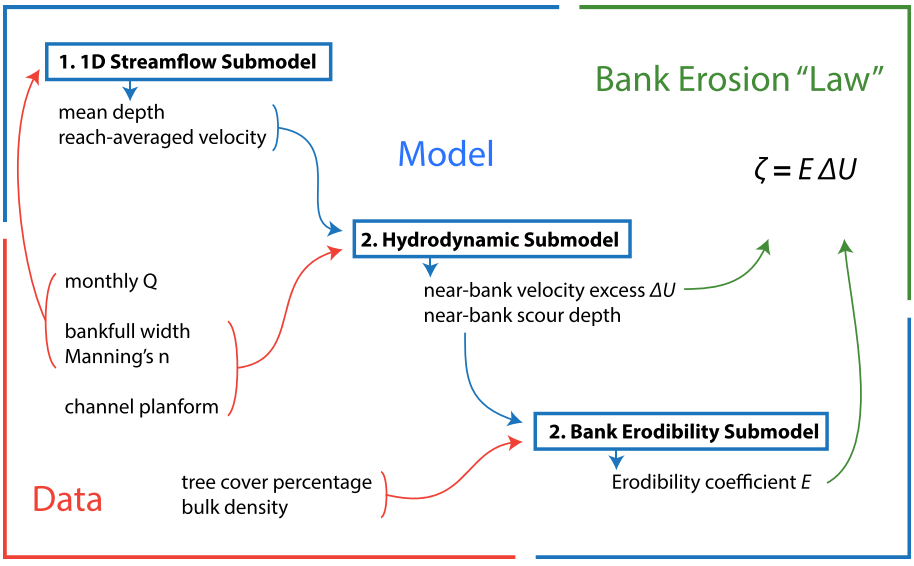

Fig. 1. Illustration of model data requirements (red), 3 main components (blue), and the geomorphic transport law used to model streambank erosion rate ζ (green).

where Q is water discharge (m^3/s) A_c is cross-sectional area (m^2), P is wetted perimeter (m), S is longitudinal slope (m/m), and n is Manning's roughness coefficient. Assuming a rectangular channel cross-section with flow of mean depth H_n and width B, then $A_c = BH_n$ and $P = B + 2H_n$. Substituting these expressions into Eq. (3) yields

$$Q = \frac{1}{n}\frac{(BH_n)^{5/3}}{(B+2H_n)^{2/3}}S^{1/2} \tag{4}$$

where, under the assumptions of steady uniform flow, H_n (m) is the depth that corresponds to a given discharge, roughness, width, and slope: the so-called normal depth. Eq. (4) can be solved for H_n using a variety of methods (Vatankhah, 2013). Here, Eq. (4) was solved using Newton's method (Tiwari et al., 2012). Monthly discharge was provided by the Noah-2.8 land surface model described below (Sexton et al., 2013). For each month, reach average velocity (m/s) was calculated as

$$U = Q^*/(BH_n) \tag{5}$$

where Q^* represents an estimate of the average monthly discharge during high flow events. Although the use of a 1-dimensional model is necessarily simplified, the hydrodynamic model only requires estimates of 1-dimensional flow variables, reach-averaged velocity U and flow depth H_n.

2.2. Hydrodynamic model

The hydrodynamic model component drives streambank erosion by providing the near-bank velocity excess ΔU (Eq. (1)). The hydrodynamic model developed by Blanckaert and de Vriend (2003, 2010) was chosen because, unlike other reduced-order models, it does not assume mild curvature or weak curvature variations (Ottevanger et al., 2012). Because hydrodynamic models built on mild-curvature

Table 1
Sources of data inputs for the streambank erosion model.

Model input		Units	Reference	Data source
Monthly time series				
*Streamflow	Q_m	m^3/s	Xia et al. (2012)	NLDAS-2, Noah-2.8 model
*Storm frequency	f_m	-	Rossi et al. (2016)	PRISM
*Event discharge	Q^*	m^3/s		Q_m/f_m
*Mean flow depth	H	m		Manning's equation
Time-constant				
*Mean depth	H_0	m	Metcalf et al. (2009)	Regional curves
*Width	B	m	Metcalf et al. (2009)	Regional curves
*Friction factor	$C_{f,0}$	-	Arcement and Schneider (1989)	Table 3
*Channel slope	S	m/m		Extracted from DEM
†Curvature	R^{-1}	m^{-1}	Güneralp and Rhoads (2007)	USGS NED 3m
†Tree cover	TC	%	Sexton et al. (2013)	USGS NED 3 m
†Bulk density	BD	g/cm^3	USGS Data Series 866	SSURGO
Scour factor	A	-		Assumed const. = 3

*Reach-averaged. †Spatially variable at the reach scale.
NLDAS-2: National Land Data Assimilation Systems (https://ldas.gsfc.nasa.gov/nldas/).
PRISM: PRISM Climate Group, Oregon State University (http://prism.oregonstate.edu).
USGS NED 3m: National Elevation Dataset, 3 m per pixel (https://datagateway.nrcs.usda.gov/).
GLCF: Global Land Cover Facility, The University of Maryland (www.landcover.org).
SSURGO: Soil Survey Geographic Database (USDA). (https://dx.doi.org/10.3133/ds866).

Please cite this article as: M. McMillan, Z. Hu, A watershed scale spatially-distributed model for streambank erosion rate driven by channel curvature, Geomorphology (2016), http://dx.doi.org/10.1016/j.geomorph.2017.03.017

assumptions can overestimate the effects of secondary flow in sharp bends (Ottevanger et al., 2012), the model of Blanckaert and de Vriend (2010) was considered more appropriate for the study area, where sharp bends are common (Fig. 5). Source code for this model has been provided by Ottevanger et al. (2013) through the OpenEarth repository (https://publicwiki.deltares.nl/display/OET/OpenEarth).

In the hydrodynamic model of Blanckaert and de Vriend (2010), hereafter referred to as the BdV model, the downstream velocity width-distribution, which leads to near-bank velocity perturbations, is parameterized by α_s/R, where $\alpha_s = -1$ corresponds to a potential vortex distribution and $\alpha_s = 1$ to a forced vortex distribution. In straight reaches, α_s is near zero and near-bank velocity is close to the average velocity (Blanckaert and de Vriend, 2003). The streamwise development of α_s/R is represented by a relaxation equation. The relaxation equation has an adaptation length largely controlled by $C_f^{-1}H/R$, and driving mechanisms representing transverse slope, curvature forcing, secondary flow, and velocity redistribution by the secondary flow (Blanckaert and de Vriend, 2010, Eqs. 35–37) . Near-bank depth excess Δh (m) is induced by basal scour and is given by $\Delta h = HA/R$, where the A/R term parameterizes transverse bed slope. The streamwise development of A/R is represented by a relaxation equation with an adaptation length dependent on H and C_f (Blanckaert and de Vriend, 2010, Eq. 20) .

Natural rivers show variability in the scour factor A, but a typical range of 2.5 to 6 is often cited (e.g., Ikeda et al., 1981; Ottevanger et al., 2012), or A is treated as a calibration parameter (Odgaard, 1987). In this model, A was assumed a constant value of 3. Although our field data do not allow characterization of A throughout each reach, the average value of A measured from individual cross-sections was 2.9, which supports our estimated constant value of 3. Modeled bed topography was initialized before beginning the simulations by setting $A = 3$ and allowing A/R to adjust to bankfull flow conditions. A was then kept constant throughout monthly simulations. Assuming a constant A is a limitation of this implementation, which is designed to be applicable at the reach and watershed scale by using remotely-sensed data. If this is not a requirement, spatial variations in A can be measured in the field.

The near-bank values of ΔU (m/s) and Δh (m) were obtained throughout each reach by the following equations

$$\Delta U = U_s \frac{\alpha_s}{R} \frac{B}{2} \tag{6}$$

$$\Delta h = H \frac{A}{R} \frac{B}{2} \tag{7}$$

where U_s is the reach-averaged velocity (m/s) and H is the cross-sectional average flow depth (m) given by the 1-dimensional streamflow model (Section 2.1). Bank height was modeled as the bankfull mean depth plus the near-bank depth excess due to basal scour, $H_b = H_0 + \Delta h$. This height corresponds to the underwater portion of the bank in the BdV model and does not account for floodplain elevation. Natural streams are thus likely to have higher banks than H_b predicts. A more accurate estimate of bank height could be made by adding H_b to bank heights extracted from a high resolution digital elevation model, which would represent the subaerial portion of the banks. The data currently available do not permit this for the studied reaches. As a consequence, the bank heights of most studied reaches are under-predicted by the current model.

The BdV model assumes a linear transverse velocity profile that is equal to the reach-averaged velocity at the channel centerline. Therefore, only one bank has a positive velocity perturbation ΔU, while the opposite bank has an equally strong negative velocity perturbation. Meander migration models based on Eq. (1) have usually assumed that channel width remains constant over the simulation period (Parker et al., 2011), and thus that deposition occurs on the opposite bank to keep pace with the eroding bank. The model of this paper is concerned with monthly to annual erosion rates, and not with long-term channel evolution and meander migration. Therefore, it does not make any assumptions about the accretion of the opposite bank. Instead, ΔU is set to zero at locations where it is modeled to be negative. As a consequence of this set of assumptions, erosion is only allowed to occur where $\Delta U > 0$ and it is restricted to only one side of a given cross-section. This is a limitation of many meander morphology models, including the present one. It is worth noting, however, that the eroding bank does not necessarily correspond to the concave bank in this model; due to the BdV model's nonlinear parameterization of the flowfield and the spatial lag between curvature and velocity perturbations, the convex bank may host positive ΔU values, especially in tight bends. The BdV model was run on a monthly timestep by varying the monthly event discharge and flow depth according to the procedure detailed above. Prior to the initial model simulation of each channel, bankfull discharge and flow depth conditions were simulated to set the initial bed geometry, and this geometry was held constant throughout the subsequent monthly simulations.

2.3. Bank erodibility parameterization

The bank erodibility coefficient E of Eq. (2) was assumed to be proportional to soil erodibility, here denoted by K. Two representations of soil erodibility, K_1 and K_2, were investigated. Wynn and Mostaghimi (2006) provided an empirical equation for sandy streambank soils in southwestern Virginia expressed as a function of coarse root density and soil bulk density at the bank toe,

$$K_1 = c_0 \exp\left(c_1 \ln RD - c_2 BD^{2.5}\right) \tag{8}$$

where RD is root density, defined as the volume of coarse roots (2–20 mm in diameter) per volume of soil (cm^3/cm^3), BD is soil bulk density (g/cm^3), and K_1 is soil erodibility with units of cm/N/s (Wynn and Mostaghimi, 2006). Due to the normalization and empirical fitting of the original data by Wynn and Mostaghimi (2006), we replaced the coefficients with generic calibration constants, c_0, c_1, and c_2; the exponent of 2.5 was retained. Pizzuto (1984) and Pizzuto and Meckelnburg (1989) found that for forested streambanks, bank erodibility was not related to soil properties but was largely controlled by vegetation density. Therefore, the second representation of soil erodibility was a power function of root density RD,

$$K_2 = c_3 RD^{c_4}, \tag{9}$$

where root density is defined as the total volume of roots per volume of soil (cm^3/cm^3), and c_3 and c_4 are calibration constants. In both K_1 and K_2, RD was estimated as a function of tree cover and bank height. Because root distributions decrease exponentially with depth below the ground surface (Zeng, 2001), RD at the bank toe was modeled as a function of tree cover and bank height,

$$RD = c_5 TC^{c_6} \exp(c_7 H_b) \tag{10}$$

where TC is tree cover (the fraction of ground area covered by vegetation >5 m tall), H_b is bank height (m), and c_5, c_6, and c_7 are calibration constants. Eq. (10) assumes that all trees are growing on a flat floodplain area adjacent to the bank, and not on the bank itself, and thus underestimates the effects of trees growing directly on the bank. Two model formulas were fitted separately, one assuming $E = K_1$, and another assuming $E = K_2$ Table 2. After combining calibration constants as appropriate, these models contain 4 and 3 free parameters, respectively. The following sections detail the implementation of this model and present the results of calibrating

Table 2
Two model formulas fitted in this paper. The models differ by their parameterization of soil erodibility and number of free parameters. $\hat{\zeta}$: Modeled streambank erosion rate (m/year). *TC*: Tree cover fraction. H_b: Modeled bank height (m). *BD*: Soil bulk density (g/cm^3). $\overline{\Delta U}$: Average near-bank velocity excess (m/s).

Model formula	Bank erodibility	Free parameters*
$\hat{\zeta}_1 = a_0 \exp\left(a_1 \ln(TC) + a_2 H_b + a_3 BD^{2.5}\right) \overline{\Delta U}$	K_1 (Eq. (8))	a_0, a_1, a_2, a_3
$\hat{\zeta}_2 = b_0 TC^{b_1} \exp(b_2 H_b) \overline{\Delta U}$	K_2 (Eq. (9))	b_0, b_1, b_2
$^*a_0 = c_0 exp(c_1 lnc_5), a_1 = c_1 c_6, a_2 = c_1 c_7, a_3 = c_2$		
$^*b_0 = c_0 c_3 c_5, b_1 = c_3 c_4, b_2 = c_7 c_4$		

the model using streambank erosion rates measured over a period of 2.5 years in the northern Gulf of Mexico coastal plain.

3. Data sources and processing

3.1. Streambank erosion calibration database

Streambank erosion rates were measured during the 2014, 2015, and 2016 water-years at 30 streambank locations throughout the northern Gulf of Mexico coastal plain (Fig. 2). The study locations were selected to represent variability in channel size, geometry, and vegetation density. All channels included in this study are single-thread, meandering, sand-bed channels, the dominant channel type in the study area (Metcalf et al., 2009). A majority of studied channels (20) were Rosgen type E, which corresponds to sinuous channels with low width-to-depth ratios generally <12 (Rosgen, 1994). Rosgen type C streams were also common (7 sites), while type F (2 sites) and type G (1 site) streams, which correspond to incised channels, were relatively rare. Metcalf et al. (2009) also identified predominately type C and E streams in the study area. Only wadeable streams were studied. Drainage areas were relatively small, most being <100 km^2. Streambank characteristics measured in the field are summarized in Fig. 3.

Streambank erosion was monitored using repeated cross-profiling, which involved measuring the distance to the bank from a rebar pin placed at the bank toe (Lawler, 1993). Measurements were taken at vertical intervals of 5–50 cm, depending on bank height, and at major breaks in slope (Bangen et al., 2014). Vertical profiles were measured once per year, resulting in final streambank erosion rates averaged over approximately two years for each location. In addition to the vertical profile sections, full channel cross-sections were measured during the initial and final site visits, and were used to determine channel geometry.

Erosion rates ranged from 0 to 1.38 m/year and were heavily right-skewed, with a mean of 0.094 m/year, median of 0.027 m/year, and standard deviation of 0.26 m/year(Fig. 4). A majority of the studied streambanks (21) had low erosion rates, <0.05 m/year,

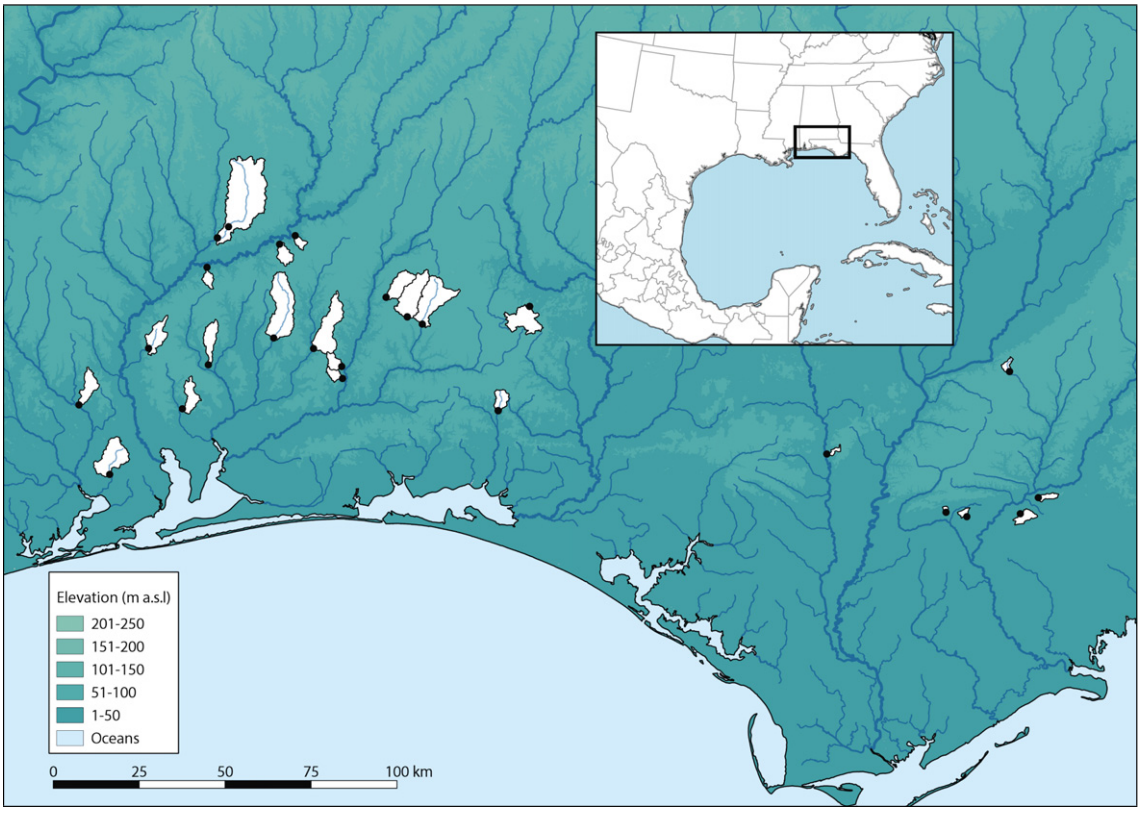

Fig. 2. Elevation map showing locations of measured streambank erosion rates (black circles) and their corresponding watershed areas (white). Inset map: Location of the study area within the northern Gulf of Mexico coastal plain.

Please cite this article as: M. McMillan, Z. Hu, A watershed scale spatially-distributed model for streambank erosion rate driven by channel curvature, Geomorphology (2016), http://dx.doi.org/10.1016/j.geomorph.2017.03.017

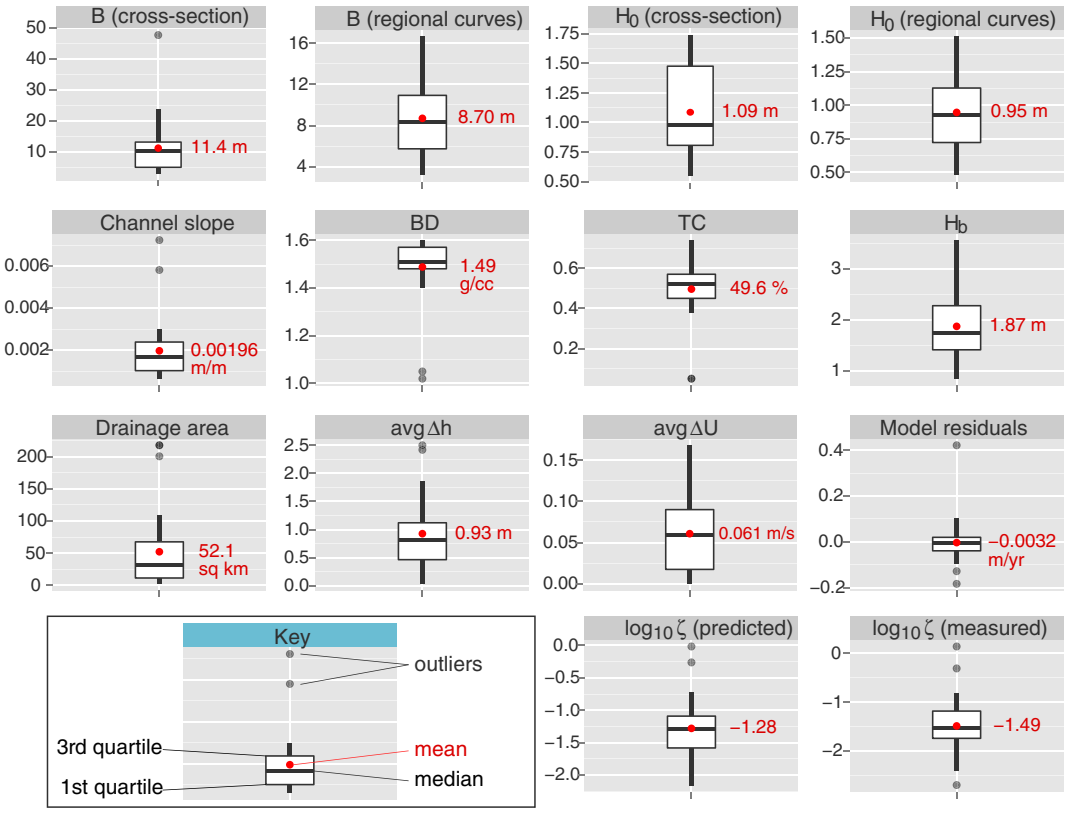

Fig. 3. Box-and-whisker plots of field measured data, model inputs, model predictions, and residuals. The whiskers extend to the largest (or smallest) observations that are within 1.5 times the interquartile range of the boxes. Outliers are data points that lie outside of the range of the whiskers. Average values refer to the average of the monthly time series at each study site. Erosion rate statistics do not include values less than or equal to zero.

including three with no measurable erosion or slight deposition. Because this paper models erosion processes and not deposition, locations that had negative erosion rates ($n = 4$) were assigned values of zero and included in the modeling. Two streambanks retreated at rates greater than 0.4 m/year; these outliers are apparent in the histogram in Fig. 4 and even on the log-transformed data in Fig. 3. Erosion rates were thus low on average but highly variable.

Because the model was designed to utilize widely available remote sensing data, rather than field data collection, no other field measurements were incorporated into model. Bankfull channel widths and depths measured at single cross-sections are included in Fig. 3 for comparison to the modeled values of width and depth obtained through regional curves as described below.

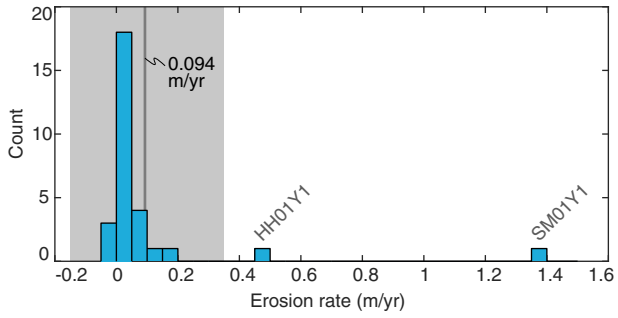

Fig. 4. Histogram of measured erosion rates, averaged over 2years, including those less than or equal to zero. Bin widths are equal to 0.05m/year. The mean (0.094m/year) is shown as the thick gray line. The shaded area represents 1 standard deviation (0.26m/year) on either side of the mean. Two outliers are labeled with identifiers that correspond to their rows in the supplementary data table.

3.2. Channel geometry data

Bankfull channel width B (m) and bankfull mean depth H_0 (m) were estimated using regional curves developed by Metcalf et al. (2009). Regional curves predict bankfull channel geometry from drainage area. Similar equations are available in many regions of the U.S.(Faustini et al., 2009; Bieger et al., 2015). In the U.S., the Natural Resources Conservation Service maintains a database of regional curve studies organized by physiographic province (NRCS, Regional Hydraulic Geometry Curves, http://www.nrcs.usda.gov/wps/portal/nrcs/detail/national/water/?cid=nrcs143_015052). If regional curves are unavailable, channel geometry can be estimated with other methods or measured in the field. For a given reach, B was held constant throughout all model simulations and H_0 was only used to set the initial bed geometry. Spatial and temporal variations in flow depth were modeled explicitly (Section 2.2).

Drainage areas were extracted from the National Hydrography Dataset (NHD) Plus v2 using the NHD Plus v2 Basin Delineator Tool. Due to heavy tree cover, channel centerlines were digitized on USGS 3D Elevation Program (3DEP) DEM (horizontal resolution 1–3 m. In less heavily-forested areas, channel centerlines can be accurately digitized using aerial or satellite imagery (Güneralp and Rhoads, 2007; Güneralp et al., 2013; Güneralp et al., 2014).

Digitized centerlines were interpolated with parametric piecewise-cubic spline (PCS) functions $X(s)$ and $Y(s)$, where s is

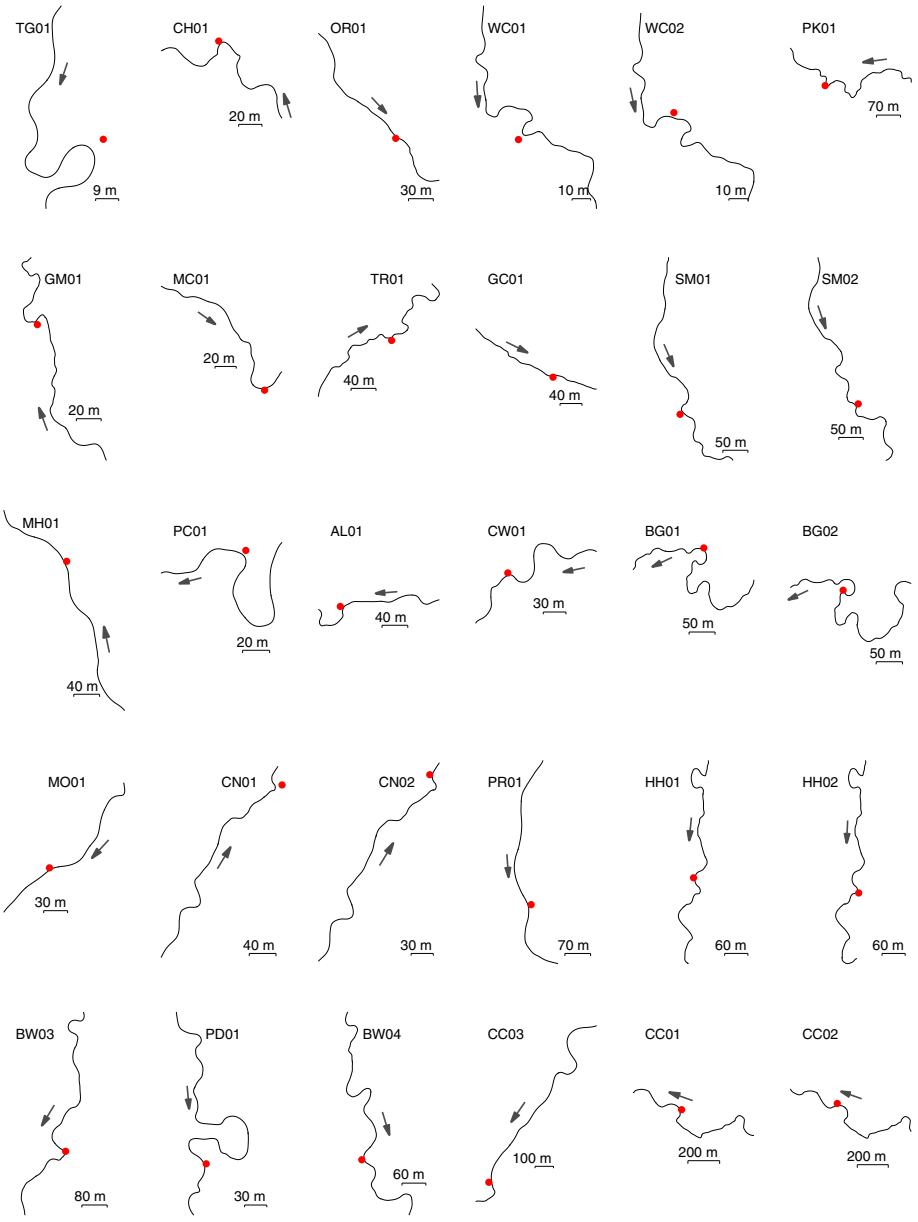

Fig. 5. Illustration of channel centerlines derived from piecewise-cubic spline interpolation. Red dots show the locations of streambank erosion monitoring sites. Arrows indicate the general flow direction.

downstream distance (m), and curvature was calculated analytically as

$$\frac{1}{R} = \frac{X'Y'' - Y'X''}{\left[(X')^2 + (Y')^2\right]^{3/2}} \tag{11}$$

where R is radius of curvature (m) (Güneralp and Rhoads, 2007). The downstream coordinate s, curvature $1/R$, and unit normal vectors n were discretized at intervals of $B/10$ meters. Fig. 5 plots these interpolated channel centerlines, which were ultimately used to train the model. Channel gradients were estimated by extracting a topographic profile along the channel centerline and robust weighted linear regression fitting. For four reaches (five individual sites) that were not resolved by the 3DEP DEM due to especially dense vegetation cover, a 50 cm DEM was created from terrestrial laser scanning (TLS) data collected during the study period. These reaches included Willacoochee Creek (sites WC01 and WC02; Fig. 6), Blue Creek (site OR01) Grab Mill Creek (site GM01), and Hollis Branch (site CH01). TLS DEMs were obtained data by taking the minimum height of each 50 cm grid cell (Fig. 6).

3.3. Monthly streamflow data

The Noah-2.8 land surface model (LSM) with National Land Data Assimilation Systems Phase 2 (NLDAS-2) forcings (Mitchell et al., 2004; Xia et al., 2012) allowed calculation of the average monthly discharge, Q_m (m^3/s), from each drainage basin. These data are available in 1/8° grid cells representing average values within each cell. This scale is similar in size to many of the watersheds in this study. Due to the coarse resolution, a pre-processing step was applied of cubic convolution downscaling to ~100 m. Q_m was computed as the sum of basin-accumulated baseflow and surface runoff during each month.

Please cite this article as: M. McMillan, Z. Hu, A watershed scale spatially-distributed model for streambank erosion rate driven by channel curvature, Geomorphology (2016), http://dx.doi.org/10.1016/j.geomorph.2017.03.017

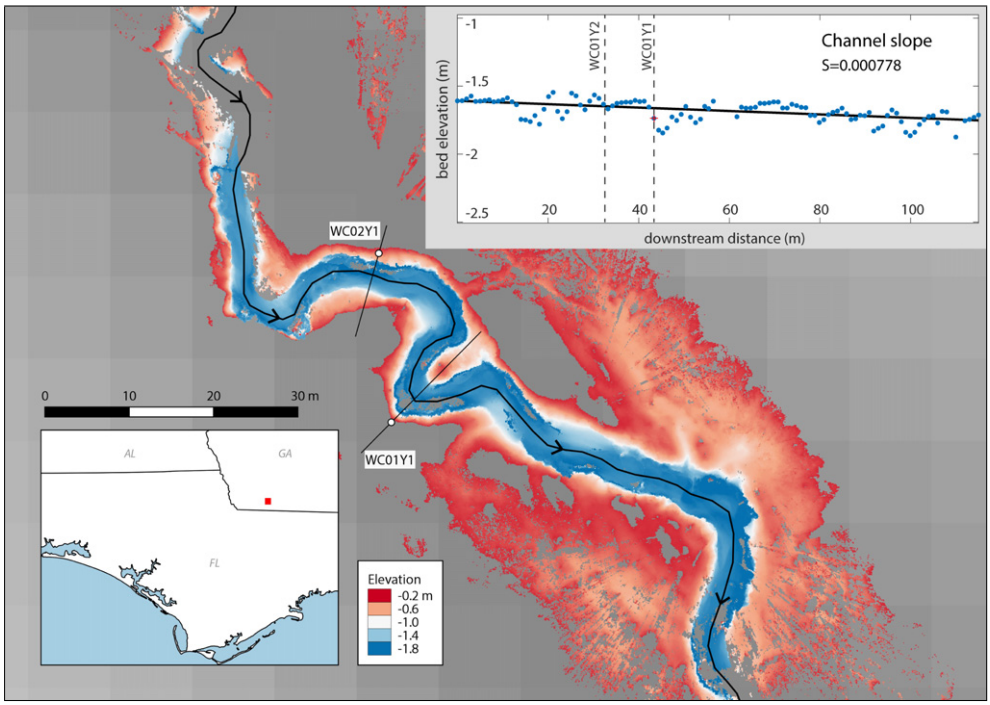

Fig. 6. Example DEM created from TLS data collected during the study period overlaid on a DEM of the highest-available resolution at the time of writing (10m National Elevation Dataset) showing two streambank erosion monitoring sites (WC01, WC02) and the digitized channel centerline (black polyline with arrows indicating flow direction). The upper right inset shows the channel profile extracted from this reach (blue dots), and the robust linear regression line used to estimate channel slope (black line) with 80x vertical exaggeration. Willacoochee Creek, SW Georgia.

Streamflow was simulated for each month by assuming a monthly event discharge, i.e., the average discharge through the channel during periods of high flow events. We assume that this event discharge is more relevant for bank erosion than average monthly or average annual discharge, which tend to be significantly lower due to long periods of baseflow. A simple method was devised to quantify the event discharge Q_m^* for each month m as $Q_m^* = Q_m/f_m$, where Q_m (m/s) is average monthly discharge, and f_m is monthly storm frequency (dimensionless). Average monthly storm frequency was calculated from daily gridded precipitation rasters from the PRISM Climate Group (www.prism.oregonstate.edu) as the ratio of wet days (>1 mm precipitation) to total days in each month (Rossi et al., 2016). Note that as storm frequency approaches one, Q_m^* approaches the average monthly discharge, and as storm frequency decreases toward zero, Q_m^* increases relative to Q. This reflects the strong effects that large, infrequent storms may have on streamflow. Q_m^* was assigned to zero for months with $f_m = 0$, though this did not occur during the study period.

3.4. Channel friction

Dimensionless channel friction is defined as the square of the shear velocity divided by average velocity,

$$C_f = \left(\frac{u_*}{U_s}\right)^2 \tag{12}$$

where $u_* = \sqrt{\tau/\rho}$ is the shear velocity (m/s), τ is average boundary shear stress (Pa), and ρ is the density of water (kg/m^3). The hydrodynamic model described below requires the dimensionless friction factor for a theoretical straight channel, $C_{f,0}$, and the extra drag induced by meandering is simulated by the hydrodynamic model itself. Therefore, Eq. (12) is written in terms of Manning's roughness coefficient n,

$$C_{f,0} = \frac{gR_hS}{U_s^2} = g\left(\frac{n}{R_h^{1/6}}\right)^2 \tag{13}$$

which allows straight channel roughness to be calculated by assuming a constant n. The hydrodynamic model assumes a trapezoidal channel cross-section (rectangular in straight reaches), which allows the hydraulic radius R_h to be calculated as $BH_0/(B + 2H_0)$.

Sefick et al. (2015) report that n can be estimated using three general approaches: consulting a table relating n to qualitative channel characteristics, comparing studied channels to photographs of channels where n has been measured, or using empirical relationships based on hydraulic variables. The difficulties in empirically estimating n have been well documented, especially for sand bed channels, where the roughness associated with bedforms changes with discharge (Ferguson, 2010). It is also difficult to account for the large roughness elements introduced by dense vegetation using empirical relationships based on grain size and other bed parameters. As an alternative, semi-quantitative approach, n can be estimated as the sum of five components times a sinuosity factor m,

$$n = m(n_b + n_1 + n_2 + n_3 + n_4) \tag{14}$$

where n_b is a base coefficient for a given boundary material, and m ranges from 1 to 1.3 to account for the increased drag of meandering channels (Arcement and Schneider, 1989). Table 3 gives estimates for n_b and n_1 through n_4 used in this study. For n_b, a base value representing bed material roughness, we assumed a median grain diameter of 0.2 mm, corresponding to fine sand, based on our qualitative

Table 3
Values used to calculate Manning's n for a theoretical straight channel. D_{50} is median grain diameter. BdV: Blanckaert and de Vriend (2010).

Component	Modeled value	Meaning
n_b	0.012	Sand bed with $D_{50} \sim 0.2$ mm
n_1	0.01	Moderate–severe surface irregularity
n_2	0.015	Frequently alternating cross-section
n_3	0.02	Minor obstruction ($< 15\%$ channel area)
n_4	0.03	Large amount of vegetation
m	1.0	Sinuosity $= 1$ (for BdV model)
n	0.087	Manning's n in this model

observations of grain size during field work. The other components, which are semi-quantitative, are also estimated based on field experience. This results in a characteristic value of $n = 0.087$ for a straight channel (letting $m = 1$). This value was assumed constant throughout the study area and corresponds to $C_{f,0}$ values around 0.05–0.11, which are significantly larger than the values for rivers reported by Ottevanger et al. (2012) , but representative of the sharp, narrow, highly vegetated channels in the study area (Thorne and Furbish, 1995). Eq. (14) assumes that n is constant for all discharges, does not account for bedform drag, and is based on semi-quantitative estimations of vegetation density, surface irregularity, and channel obstruction, and thus amounts to an order of magnitude estimate.

3.5. Soil erodibility data

Soil erodibility was modeled using K_1 (Eq. (8)) and K_2 (Eq. (9)). Area- and depth-weighted average bulk density was obtained from the SSURGO dataset in the form of a 10 m raster (Wieczorek, M. E., USGS Data Series 866, http://water.usgs.gov/GIS/metadata/usgswrd/XML/ds866_ssurgo_variables.xml).

Root density RD was modeled as a function of tree cover TC and bank height H_b (Eq. (10)). Tree cover was obtained as a 30 m raster from the Global Land Cover Facility at the University of Maryland, which represents the fraction of each 900 m^2 pixel covered by vegetation greater than 5 m in height (Sexton et al., 2013). This dataset is based on Landsat observations, is free to the public, covers the entire globe, and is readily available online (http://www.landcover.org/data/landsatTreecover/). Three datasets are available based on observations from 2000, 2005, and 2010. Although erosion rates were measured during 2014–2016, the 2010 dataset contains many small gaps associated with cloud cover. Therefore, the 2005 dataset was used. Although the 2005 tree cover dataset is approximately 10 years out of date, it is highly unlikely that any of the small headwater streams investigated in this study have shifted significantly at the 30 m/pixel scale since 2005. The largest erosion rate observed in this study, ~1.3 m/year, corresponds to a total lateral shift of 13 m over 10 years, assuming that such a high erosion rate is sustained over the 10 year period. Additionally, no major forest disturbances were observed at any of the study sites, which would be obvious had they occurred during the last 10 years in the study area. Most studied streambanks hosted trees of varying species and diameters, which qualitatively supports the moderately high values of tree cover exhibited in the 2005 dataset. Most sites hosted trees greater than 30 cm in diameter, which indicates that they have been growing for much longer than 10 years. One exception is Sconnier's Mill Creek (sites SM01 and SM02), which has recently lost much of its tree cover in a limited area near the bank. Based on our field experience, an estimated value of 5% was assigned as input for this location. All other locations used values from the 2005 tree cover dataset. If this model is applied in more dynamic environments in the future, the 2005 tree cover dataset may prove to be inadequate, in which case the 2010 dataset may be used, or tree cover may be estimated using different methods.

3.6. GIS environment

The raster data representing tree cover, bulk density, and monthly streamflow and the polylines representing channel geometry were managed in a geographic information system (GIS) using Matlab (Fig. 7). The 30 m pixel size of these raster data is relatively coarse compared to the studied channel reaches. Errors can arise if the raster data are sampled at pixels representative of the opposite streambank or corresponding to the mid-channel open water. Therefore, rasters were sampled at bank locations, rather than channel centerlines. Left- and right-bank locations were modeled as one channel width from each centerline using the unit normal vectors n calculated during PCS-interpolation of the channel centerline. To associate measured erosion rates to a modeled bank location and channel centerline node, the GPS locations recorded in the field were matched with the nearest-neighbor bank location (Fig. 7).

Rasters were sampled at runtime by looping through the bank point locations and extracting (Matlab function *imread*) and interpolating the four nearest pixels from the raster dataset. This approach has the advantage that rasters of differing resolution and/or spatial references can be used without the need to reproject the entire raster, provided that geotransforms exist between the various spatial reference coordinates. This allows entire river reaches to be modeled efficiently. Bilinear interpolation results in bank erodibility estimates that vary smoothly throughout a meander bend, rather than in sharp jumps characteristic of the raw raster pixels. Each bank location, therefore, is assigned unique values of tree cover and bulk density as well as a value of near-bank velocity excess and bank height from the hydrodynamic model.

3.7. Regression analysis

Given the model structure presented above and the model formulas of Table 2, the free parameters must be estimated by minimizing model error. There are at least three straightforward options, however, each with its own set of assumptions regarding error structure. Letting $f(x)$ represent an arbitrary, nonlinear function of independent variables, erosion rate ζ can be modeled as

$$\zeta = f(x) + \epsilon \tag{15}$$

$$\zeta = f(x) \cdot \epsilon \tag{16}$$

$$\zeta = f(x) \cdot \exp(\epsilon) \tag{17}$$

where ϵ is normal error, $\epsilon \sim \mathcal{N}(0, \sigma)$. Eq. (15) assumes that error is additive and normally distributed, Eq. (16) assumes that error is multiplicative and normally distributed, and Eq. (17) assumes that error is multiplicative and lognormally distributed (Xiao et al., 2011). It is worth noting that Eq. (17) results from log-transforming both sides of a nonlinear equation, e.g., a power-law relationship, which is commonly done to linearize the equation for practical or scientific reasons (Xiao et al., 2011). The choice of error model can often have a large impact on the final values of regression parameters and thus also on the conclusions drawn from modeling studies.

We investigated all three error models while calibrating the free parameters. Normal additive and normal multiplicative error models were investigated through nonlinear regression (Matlab function *fitnlm*); lognormal multiplicative error was investigated by log-transforming the data for the equations given in Table 2 and linear regression of the log-transformed data. Only the normal multiplicative error model (Eq. (16)) resulted in accurate predictions of streambank erosion rate. Additionally,

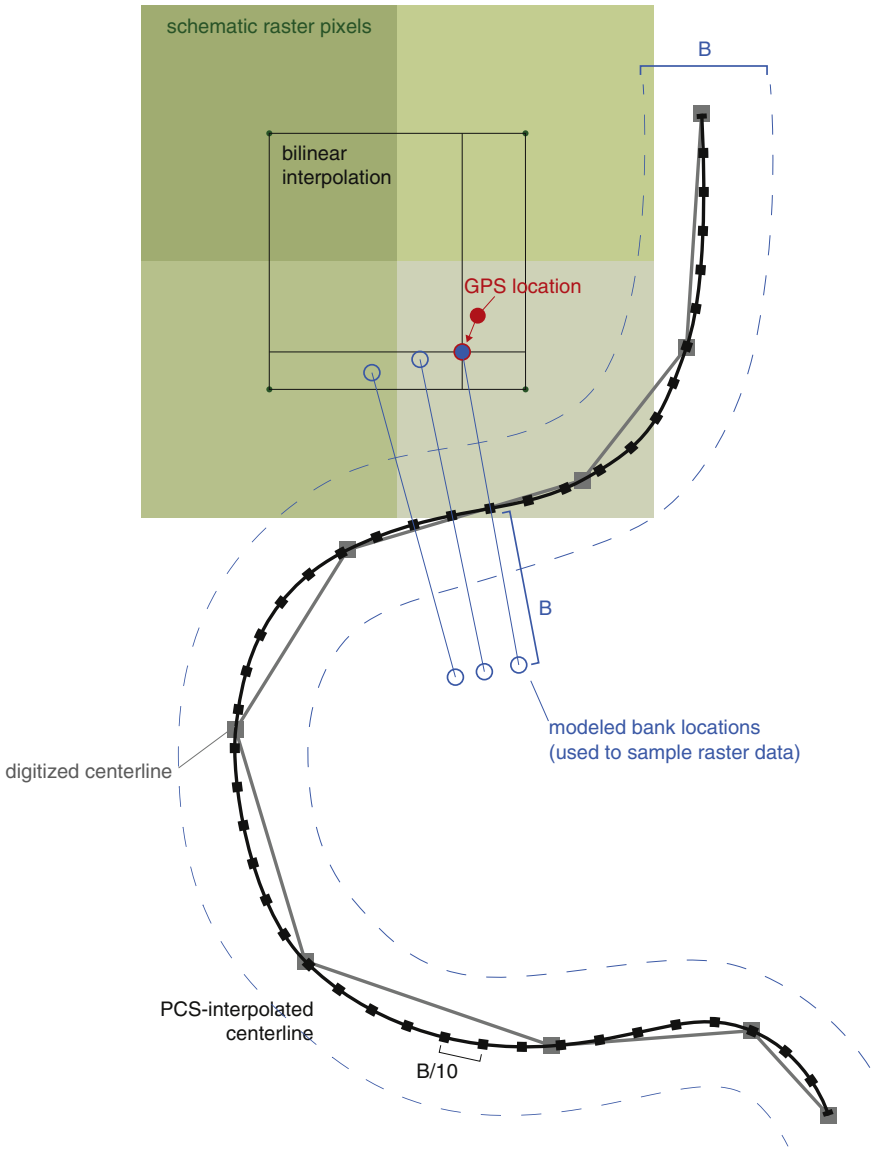

Fig. 7. GIS environment. Centerlines digitized on a 3 m DEM (gray polyline) were PCS-interpolated (black). Banks locations (blue circles) were assumed B meters (channel width) from the centerline. The bank point nearest the cross-section as surveyed in the field (red circle) was selected. The 4 nearest raster pixels were interpolated (green squares).

for stochastic events such as streambank erosion, variance is proportional to the maximum magnitude of individual events (Pizzuto et al., 2010), which we interpret as further evidence that a regression model with proportional error variance is most appropriate.

In the context of nonlinear regression, R^2 is reported as the square of the Pearson correlation coefficient R of the actual and modeled values. However, the streambank erosion rates reported here were not normally distributed (Fig. 4), and two outliers will have a large influence on the regression statistics. Because these outliers are due to naturally high erosion rates and not to measurement error, we did not remove them from the dataset, especially because the model is designed to predict streambank erosion hotspots such as these. As a consequence, parametric statistics such as R and R^2, which are not robust to outliers, are misleading. Therefore, we also report a more robust measure of correlation, Spearman's rank correlation coefficient, ρ, which is equal to the Pearson correlation coefficient of the rank values of actual and modeled streambank erosion rates. Although ρ cannot be interpreted as easily as R or R^2, it is useful in comparing models from the same dataset.

4. Results

Two separate models were run using the same input data: one with soil erodibility as K_1 and another with soil erodibility as K_2. Fig. 9plots the results of statistical calibration of each model. For $E = K_1$, the fitted equation is given by

$$\hat{\zeta}_1 = 0.0322 \exp\left[-1.030 \ln(TC) + 0.197 H_b + 0.768 BD^{2.5}\right] \overline{\Delta U}. \quad (18)$$

Soil erodibility modeled by K_1 was thus predicted to be inversely related to tree cover and directly related to bank height and bulk density. In contrast to this result, Wynn and Mostaghimi (2006) reported a strong inverse relationship to bulk density. Possible reasons for this discrepancy are discussed below.

The simpler model incorporating $E = K_2$, in which soil erodibility is a function of bank height and tree cover only, is given by the fitted equation,

$$\hat{\zeta}_2 = 0.294 TC^{-1.05} \exp(0.157 H_b) \overline{\Delta U} \quad (19)$$

Please cite this article as: M. McMillan, Z. Hu, A watershed scale spatially-distributed model for streambank erosion rate driven by channel curvature, Geomorphology (2016), http://dx.doi.org/10.1016/j.geomorph.2017.03.017

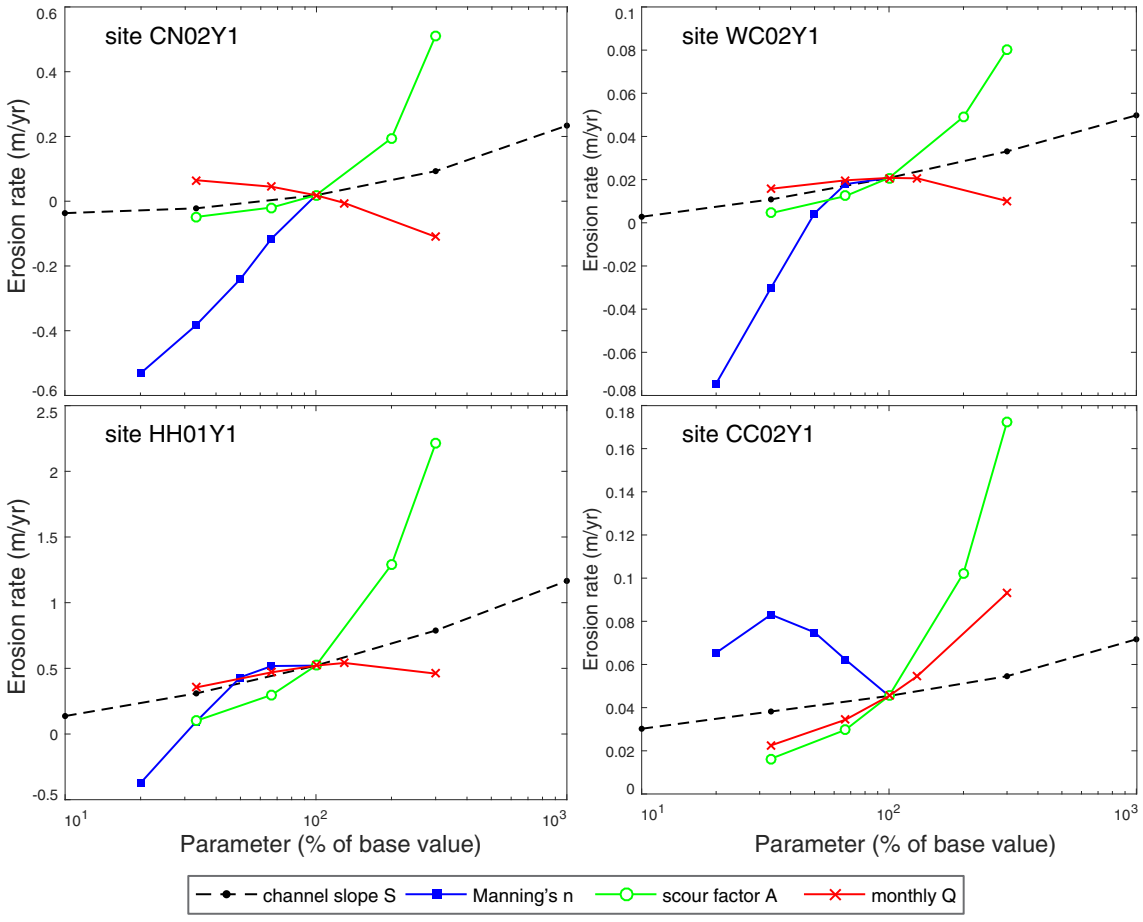

Fig. 8. Sensitivity of the modeled streambank erosion rates to 4 model parameters: channel slope *S*, Manning's *n*, scour factor *A*, average discharge *Q*. Changes in erosion rates resulting from changing each of these parameters independently are plotted for four study sites. The parameters are expressed as percentages of their base values discussed in the text.

which suggests that bank erosion rates are directly related to near-bank velocity excess and bank height and inversely related to tree cover. According to the root density parameterization (Eq. (10)), the exponent of *TC* and the coefficient of H_b are expected to be opposite in sign, since root density at the bank toe should increase with tree cover and decrease with bank height. The coefficients and exponents are thus physically sound if streambank erosion is inversely related to root density. Although the data points with measured streambank erosion rates equal to zero ($n = 4$) are not shown on the log-log plots of Fig. 9, they were also predicted by the models. Both models predicted erosion rates of zero for two of the four, i.e., $\overline{\Delta U} < 0$. The model incorporating K_1 predicted the other two to erode at 0.0079 m/year and 0.047 m/year, a modest overestimate of ~1 to 5 cm/year. The model incorporating K_2 predicted negligible values of less than 0.001 m/year for these two locations.

Fig. 8 plots the model's sensitivity on four parameters with significant uncertainty: channel slope *S*, Manning's *n*, scour factor *A*, and monthly discharge Q_m. Parameters were varied as percentages of their base values. For *n* and *A*, base values were constant for all sites (0.087 and 3 respectively, described above). For *S* and Q_m, the base base values are reach-averaged values. Sensitivity analyses for all calibration sites followed similar patterns, illustrated in Fig. 8. The model's response to Manning's *n* variations, which ranged from 0.0174 to 0.087, showed the most variability. In all cases, as *n* decreased, high velocity zones progressively shifted onto the inner, rather than the outer banks. We interpret this as a sign that the lowest *n* values investigated in the sensitivity analysis were not physically realistic for the study reaches. A site's response to changes in *n* depended on the its location with respect to its meander bend and to adjacent bends. The model's response to variations in monthly *Q* was similarly variable across sites due to their locations in meander bends. Larger values of *Q* correspond to lower channel friction (Eq. (13)) and larger flow depths, both of which increase the spatial lag between curvature forcing and velocity perturbations (Blanckaert and de Vriend, 2010). The model's response to variations in *S* and *A* was consistent across all study sites, with *A* having a larger effect on model output (Fig. 8).

This simple sensitivity analysis suggests that the model is most sensitive to changes in Manning's *n* and to the scour factor *A*. Future applications of the model could be improved by incorporating spatial variability into these parameters, rather than the constant values we have assumed here.

Fig. 10 shows the results of applying the model with $E = K_2$ to a medium-sized stream in a mixed pasture/forest landscape in Okaloosa County, FL. The simulation was run using the same input data used to train the model, including a monthly discharge time series of 24 months. A few bends are currently meandering out of the riparian buffer zone into pastured areas, where tree cover is very low. High erosion rates of >0.75 m/year were predicted on the non-forested section of the large bend downstream (south) of the calibration locations (HH01 and HH02), and rates of almost 1 m/year were modeled on a tight, non-forested bend in southern part of the map. The non-forested bends all host erosion rates of well over 0.25 m/year. Reasonably high erosion rates were not only confined to non-forested bends, however; several sharp bends in the forested portion of the image were predicted to erode up

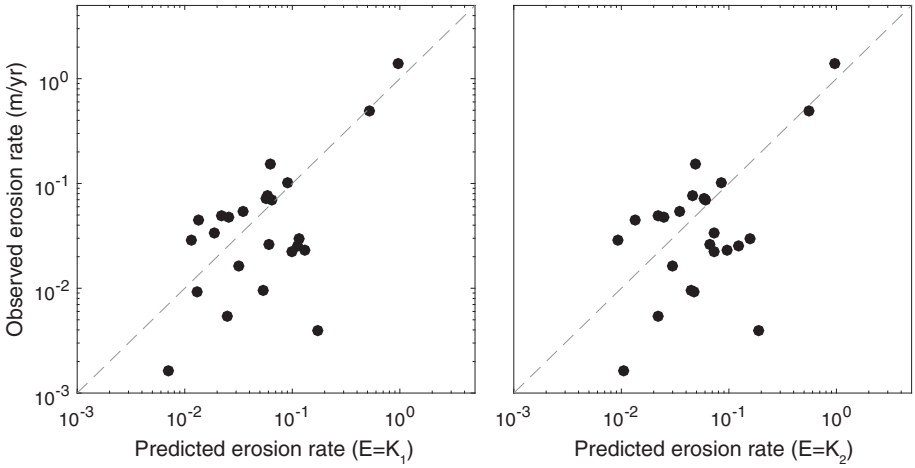

Fig. 9. Results of model calibration using soil erodibility parameters K_1 (Eq. (8)) and K_2 (Eq. (9)). The model with K_1 predicts streambank erosion rates with a significant correlation ($R^2 = 0.91$, $p < 0.001$, $\rho = 0.53$). The model with K_2 predicts streambank erosion rates to a similar degree ($R^2 = 0.90$, $p < 0.001$, $\rho = 0.48$) but with fewer parameters. The dashed line is 1:1 correlation. Here, R^2 represents the square of the Pearson correlation coefficient R between modeled and predicted erosion rates in their original units; ρ is Spearman's rank correlation coefficient. See the text for discussion on interpreting these statistics for this dataset.

to 0.25 m/year, comparable to the non-forested bend near HH01. The moderate erosion rates on these forested bends are associated with increased basal scour resulting from their high curvatures. Additionally, the upstream geometry of the meander train could have a cumulative downstream effect on erosion rates, as shown by Güneralp and Rhoads (2009, 2010). The bottom panel plots channel curvature (B/R), velocity excess ($\Delta U/U$) and depth excess ($\Delta h/H$) against the downstream coordinate s and shows the spatial lag between curvature and the velocity perturbations. Fig. 10 illustrates the model's ability to predict streambank erosion rates throughout a 1 km reach displaying high variability in tree cover and channel geometry characteristics.

5. Discussion

We presented two models that predicted streambank erosion rates (Fig. 9). While both are highly correlated to observed erosion rates, the model incorporating K_2 for soil erodibility contains only three free parameters, while the model incorporating K_1 contains four. The negative relationship between bulk density and bank erosion reported by Wynn and Mostaghimi (2006) was not observed here. This could be due to many factors. Soils with high organic matter and root biomass content would express lower bulk densities despite being less erodible overall, and sandy soils commonly express higher bulk densities as well as higher erodibility. The large-scale SSURGO dataset may also be unable to resolve the spatial heterogeneity of bank materials, especially for many of the small channels used to calibrate the model. This result agrees with recent work by Daly et al. (2015), who found that watershed-scale relationships for bank erodibility based on soil properties showed no significant correlations to erodibility coefficient or critical shear stress. It is therefore not surprising that K_1 did not improve the bank erodibility estimation across the many watersheds of our study.

The overall effectiveness of K_2 agrees with the observations of Pizzuto (1984), Pizzuto and Meckelnburg (1989), and Pizzuto et al. (2010), who found that forested streambank erodibility is largely controlled by tree density. Assuming representative values of tree cover of 5–10% for pastured/agricultural areas and 40–60% for forested areas, Eq. (19) predicts that forested streambanks retreat 4–12 times slower than non-forested ones. This generally agrees with previous studies, which have reported two to five-fold differences

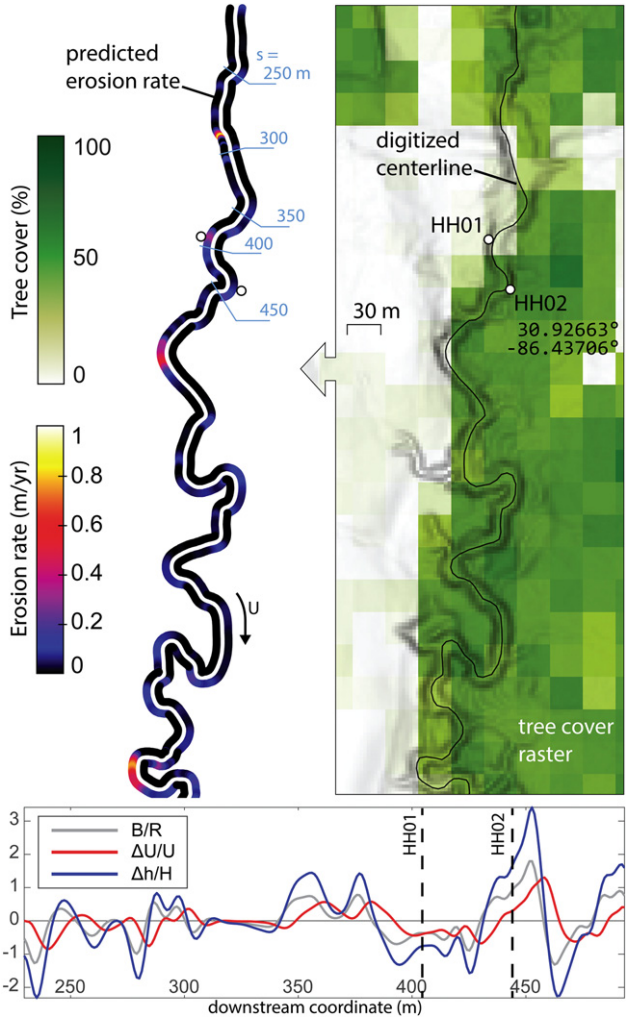

Fig. 10. Model application on Horsehead Creek (sites HH01 and HH02). Right: Input tree cover dataset (white to green) and channel centerline digitized on 3 m DEM (shown with slope shaded). Left: Modeled streambank erosion rates throughout the reach. Light blue numbers map the downstream coordinate plotted in the bottom panel. Flow is north to south. Bottom: Comparison of curvature (B/R), velocity excess ($\Delta U/U$), and depth excess ($\Delta h/H$) during the December 2015 simulation.

Please cite this article as: M. McMillan, Z. Hu, A watershed scale spatially-distributed model for streambank erosion rate driven by channel curvature, Geomorphology (2016), http://dx.doi.org/10.1016/j.geomorph.2017.03.017

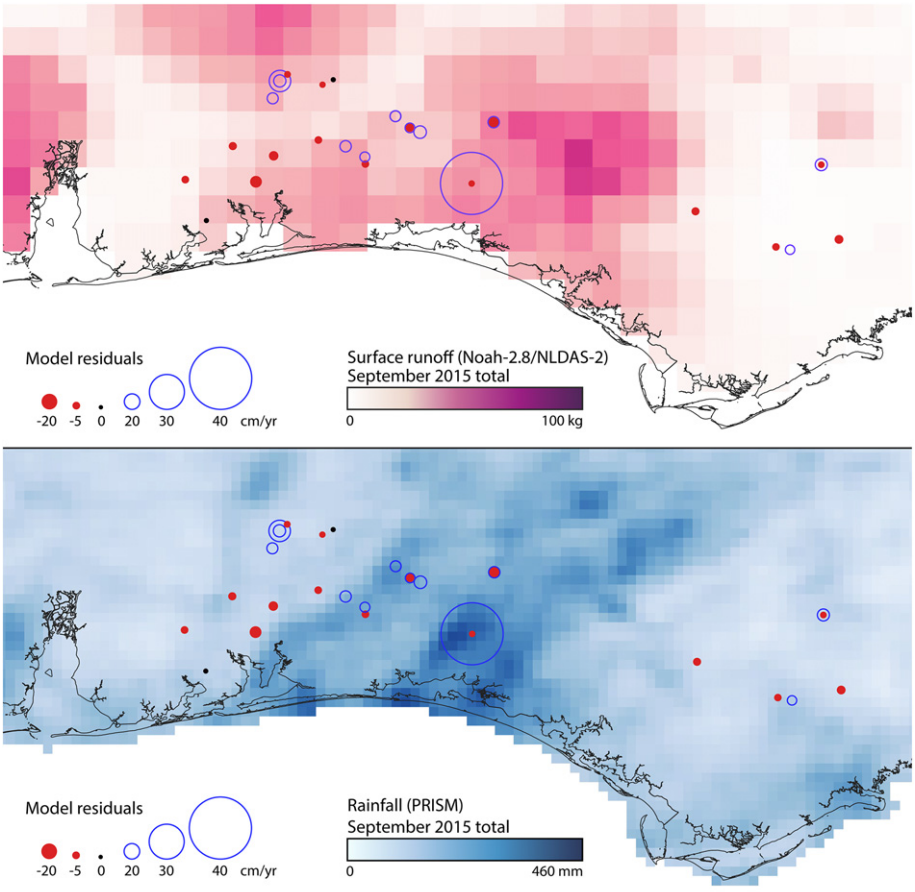

Fig. 11. Map of residuals. Comparison of Noah-2.8 surface runoff (top) and PRISM precipitation (bottom) for September 2015 demonstrates discrepancies in the Noah model. A small but intense storm near the middle of the map is not represented in the surface runoff data.

in bank erodibility between forested and non-forested streambanks (Micheli et al., 2004; Allmendinger et al., 2005; Sass and Keane, 2012). The relatively large (up to 12-fold) difference implied here is probably due to the extremely low erosion rates of forested streambanks in these low-gradient coastal plain streams, rather than especially high erosion rates of non-forested streambanks.

In both models, there appear to be two distinct groups of data points, one with largely positive residuals and another with negative residuals. Residuals were mapped and Moran's Index of $I = -0.09$ was calculated in ArcMap, indicating that the residuals are not spatially autocorrelated and are not statistically different from random ($p = 0.86$). Fig. 11 maps the residuals over Noah-2.8 surface runoff and PRISM precipitation totals for September 2015. Comparison to the PRISM data shows that some highly localized but intense storms were not represented well in the Noah-2.8 runoff simulations, either as a result of the coarse resolution of the NLDAS-2 forcing data, or because of inaccuracies in the Noah-2.8 LSM. Extreme rainfall totals and flash flooding were documented by weather stations in the area during this event (National Weather Service, North Central Gulf Coast Heavy Rain Event 27-29 September 2015, accessed 16 June 2016, https://www.weather.gov/mob/heavyrain_sep2015). It is likely that the Noah-2.8 underestimated surface runoff during such small intense storms, which may have contributed to the negative residuals shown on the map (Fig. 11).

It would be useful to compare the model of this paper to similar models in the literature, but few if any comparable models exist. We therefore fit two simple models for comparison: a purely empirical statistical model and an Ikeda-type model based on Eq. (2) with a spatially constant erodibility coefficient E. All models were fit using the nonlinear regression procedure outlined in Section 3.7. Table 4 shows that the model of this paper, using either K_1 or K_2, outperforms these simpler models according to Spearman's rank correlation coefficient ρ, which is robust to outliers. R^2 is reported as the square of the correlation coefficient between the predicted and actual streambank erosion rates, but is skewed by outliers. The negative exponents on slope and drainage area exhibited by the purely empirical model are likely not physically sound, and $\rho < 0$ indicates an overall negative relationship to erosion rates. The Ikeda-type model is positively correlated to erosion rates, but this correlation is not as strong as the models proposed here. This comparison illustrates the utility of combining the BdV hydrodynamic model with a spatially distributed bank erodibility relationship.

An existing spatially distributed model for total sediment yield from drainage basins, SedNet, quantifies annual streambank erosion as a function of bankfull stream power, bank erodibility, and a daily

Table 4
Comparison of the model of this paper with a purely empirical model and a model lacking spatial variability in bank erodibility (an Ikeda-type model based on Eq. (1)).

Model	Description	Statistics
Eq. (18)	This paper, K_1	$R^2 = 0.91, \rho = 0.53$
Eq. (19)	This paper, K_2	$R^2 = 0.90, \rho = 0.48$
$\hat{\xi} = 0.032BD^{-5.4}S^{-0.037}A^{-0.86}TC^{-2.8}$	Empirical model	$R^2 = 0.98, \rho = -0.20$
$\hat{\xi} = 1.54\tilde{\Delta U}$	Eq. (2)	$R^2 = 0.034, \rho = 0.25$

Please cite this article as: M. McMillan, Z. Hu, A watershed scale spatially-distributed model for streambank erosion rate driven by channel curvature, Geomorphology (2016), http://dx.doi.org/10.1016/j.geomorph.2017.03.017

streamflow factor (Wilkinson et al., 2009, 2014). The SedNet model requires a long-term dataset of daily streamflow observations as well as two raster datasets: one representing vegetation cover (values of 0 to 1, with 1 representing fully intact riparian vegetation) and another of bank erodibility (values of 0 or 1, with 0 representing bedrock and 1 representing pixels characterized as soil). Rather than modelling the spatial variability introduced by hydrodynamic processes, SedNet models the average bank erosion of entire stream links. SedNet was not designed to allow the prediction of local streambank erosion rates, or the identification of erosion hot-spots, but rather to simulate the large-scale processes exporting sediment from large drainage basins; streambank erosion is just one part of the model. Nevertheless, it is increasingly being used to estimate local streambank erosion rates because it is the only spatially distributed model that attempts to do so (Bartley et al., 2008). One recent evaluation of the accuracy of the streambank erosion rates predicted by SedNet showed that its original predictions differed from measured erosion rates (averaged over 10 locations) by a factor of 74, but this discrepancy was decreased to a factor of ~2 with calibration to field-measured values of bed slope and bankfull discharge.

The main goal of this paper was to develop a spatially distributed model that incorporated widely available data and could be readily used in practical applications. This approach necessitated a few simplifications. Meander migration models based on Eq. (1) usually assume a constant discharge to determine ΔU, e.g., mean annual Q, bankfull Q, or another statistic (Camporeale and Ridolfi, 2010). Here, we computed a monthly-varying discharge statistic $Q*$, and ran the BdV model on this timestep before averaging the monthly estimates of ΔU. This approach was designed to account for variability in precipitation and runoff at the regional scale, and for increased erosion during high flow periods. This is a novel application of Eq. (1), however, and it has not been shown that streambank erosion rates are proportional to ΔU on these shorter timescales.

The sensitivity analysis showed that the model is sensitive to errors in Manning's roughness coefficient n and the scour factor A, but these parameters are difficult to estimate using only remotely sensed data, or other widely available datasets. We assumed characteristic values for these parameters and held them constant throughout the study area. This is a major limitation of the model and likely a source of error. In the future, reach-scale measurements of n and A should be incorporated into the model.

Another limitation of the model is its reliance on an *ad hoc* method for determining the relevant monthly discharge, which was estimated as a function of average monthly discharge and storm frequency. The lack of streamgauges in the basins being studied necessitated modeling of monthly streamflow. The average monthly streamflow estimates are from the Noah-2.8 LSM, a large-scale land surface model designed to simulate processes acting at the global, continental, and large watershed scale. Such models have been shown to be relatively inaccurate at predicting streamflow in small basins, though they often express a higher skill in the southeastern U.S. than in other regions (Xia et al., 2012).

A thorough validation of this model is outside the scope of this paper, but should be done at the reach and watershed scales. The model could be evaluated on a few reaches where channel geometry is known or can be easily measured. Existing streambank erosion rate databases could be useful for model validation, provided that the GPS coordinates of streambank measurements can be determined accurately.

6. Conclusions

Bartley et al. (2008) remarked that "it will be difficult for catchment scale sediment budget models to ever accurately predict the location and rate of bank erosion due to the variation in bank erosion rates in both space and time." de Vente et al. (2013) cited the lack of a bank erosion component as a major limitation of current sediment detachment models. We presented a spatially distributed model for streambank erosion incorporating an empirical soil erodibility parameter (K_2), a nonlinear hydrodynamic model, and monthly discharge forcings. An application of the model to a medium-sized stream in the Gulf Coastal plain (Fig. 10) demonstrated its potential for quantifying annual streambank erosion throughout a mixed forest/pasture reach. Although future work should focus on improving the model's parameterization of roughness and streamflow, as well as a thorough evaluation and validation of model predictions throughout multiple reaches, the current model shows a significant correlation to observed erosion rates. The model thus represents a first step toward filling the long-standing gap emphasized by Bartley et al. (2008) and de Vente et al. (2013).

Supplementary data to this article can be found online at http://dx.doi.org/10.1016/j.geomorph.2017.03.017.

Acknowledgments

We thank David Cambron and Michele Goodfellow for their help in collecting data for this study. This study was based on a work supported by a grant from the Florida Fish and Wildlife Conservation Commission and the U.S. Fish and Wildlife Service (State Wildlife Grant13058). The Geological Society of America, the Gulf Coast Association of Geological Societies, and the University of West Florida Scholarly and Creative Activities Committee provided additional funding. The authors thank Dr. Jim Pizzuto and an anonymous reviewer for their thoughtful critique of this paper. The paper was greatly improved by their comments.

References

Allmendinger, N.E., Pizzuto, J.E., Potter, N., Johnson, T.E., Hession, W.C., 2005. The influence of riparian vegetation on stream width, Eastern Pennsylvania, USA. Geol. Soc. Am. Bull. 117, 229–243. http://dx.doi.org/10.1130/B25447.1.

Arcement, G.J., Schneider, V.R., 1989. Guide for Selecting Manning's Roughness Coefficients for Natural Channels and Flood Plains. . U.S. Geological Survey Water-Supply Paper 2339U.S. Government Printing Office, Washington, DC.

Bandyopadhyay, S., Ghosh, K., De, S.K., 2014. A proposed method of bank erosion vulnerability zonation and its application on the river Haora, Tripura, India. Geomorphology 224, 111–121. http://dx.doi.org/10.1016/j.geomorph.2014.07.018.

Bangen, S.G., Wheaton, J.M., Bouwes, N., Bouwes, B., Jordan, C., 2014. A methodological intercomparison of topographic survey techniques for characterizing wadeable streams and rivers. Geomorphology 206, 343–361. http://dx.doi.org/10.1016/j.geomorph.2013.10.010.

Bartley, R., Keen, R.J., Hawdon, A.A., Hairsine, P.B., Disher, M.G., Kinsey-Henderson, A.E., 2008. Bank erosion and channel width change in a tropical catchment. Earth Surf. Process. Landf. 33, 2174–2200. http://dx.doi.org/10.1002/esp.1678.

Bieger, K., Rathjens, H., Allen, P.M., Arnold, J.G., 2015. Development and evaluation of bankfull hydraulic geometry relationships for the physiographic regions of the United States. J. Am. Water Resour. Assoc. 51, 842–858. http://dx.doi.org/10.1111/jawr.12282.

Blanckaert, K., de Vriend, H.J., 2003. Nonlinear modeling of mean flow redistribution in curved open channels. Water Resour. Res. 39, 1375. http://dx.doi.org/10.1029/2003WR002068.

Blanckaert, K., de Vriend, H.J., 2010. Meander dynamics: a nonlinear model without curvature restrictions for flow in open-channel bends. J. Geophys. Res. Earth Surf. 115, http://dx.doi.org/10.1029/2009JF001301. F04011.

Bull, L.J., 1997. Magnitude and variation in the contribution of bank erosion to the suspended sediment load of the River Severn, UK. Earth Surf. Process. Landf. 22, 1109–1123. http://dx.doi.org/10.1002/(SICI)1096-9837(199712)22:12¡1109::AID-ESP810¿3.0.CO;2\ignorespaces-O.

Camporeale, C., Perona, P., Porporato, A., Ridolfi, L., 2007. Hierarchy of models for meandering rivers and related morphodynamic processes. Rev. Geophys. 45, 5–28. http://dx.doi.org/10.1029/2005RG000185.

Camporeale, C., Ridolfi, L., 2010. Interplay among river meandering, discharge stochasticity and riparian vegetation. J. Hydrol. 382, 138–144. http://dx.doi.org/10.1016/j.jhydrol.2009.12.024.

Couper, P.R., 2003. Effects of siltclay content on the susceptibility of river banks to subaerial erosion. Geomorphology 56, 95–108. http://dx.doi.org/10.1016/S0169-555X(03)00048-5.

Crosato, A., 2009. Physical explanations of variations in river meander migration rates from model comparison. Earth Surf. Process. Landf. 34, 2078–2086. http://dx.doi.org/10.1002/esp.1898.

Daly, E.R., Miller, R.B., Fox, G.A., 2015. Modeling streambank erosion and failure along protected and unprotected composite streambanks. Adv. Water Resour. 81, 114–127. http://dx.doi.org/10.1016/j.advwatres.2015.01.004.

Dietrich, W., Bellugi, D., Sklar, L., Stock, J., Heimsath, A., Roering, J., 2003. Geomorphic Transport Laws for Predicting Landscape Form and Dynamics. In: Wilcock, P., Iverson, R. (Eds.), Prediction in Geomorphology. American Geophysical Union., pp. 103–132.

Dietrich, W., Smith, J., Dunne, T., 1979. Flow and sediment transport in a sand bedded meander. J. Geol. 87, 305–315.

Dietrich, W.E., Smith, J.D., 1983. Influence of the point bar on flow through curved channels. Water Resour. Res. 19, 1173–1192. http://dx.doi.org/10.1029/WR019i005p01173.

Eke, E., Parker, G., Shimizu, Y., 2014. Numerical modeling of erosional and depositional bank processes in migrating river bends with self-formed width: morphodynamics of bar push and bank pull. J. Geophys. Res. Earth Surf. 119, 1455–1483. http://dx.doi.org/10.1002/2013JF003020.

Faustini, J.M., Kaufmann, P.R., Herlihy, A.T., 2009. Downstream variation in bankfull width of wadeable streams across the conterminous United States. Geomorphology 108, 292–311. http://dx.doi.org/10.1016/j.geomorph.2009.02.005.

Ferguson, R., 2010. Time to abandon the Manning equation? Earth Surf. Process. Landf. 35, 1873–1876. http://dx.doi.org/10.1002/esp.2091.

Florsheim, J.L., Mount, J.F., Chin, A., 2008. Bank erosion as a desirable attribute of rivers. BioScience 58, 519–528. http://dx.doi.org/10.1641/B580608.

Gregory, K., 2006. The human role in changing river channels. Geomorphology 79, 172–191. http://dx.doi.org/10.1016/j.geomorph.2006.06.018.

Güneralp, İ., Filippi, A., Hales, B., 2013. River-flow boundary delineation from digital aerial photography and ancillary images using Support Vector Machines. GISci. Remote Sens. 50, 1–25. http://dx.doi.org/10.1080/15481603.2013.778560.

Güneralp, İ., Filippi, A.M., Randall, J., 2014. Estimation of floodplain aboveground biomass using multispectral remote sensing and nonparametric modeling. Int. J. Appl. Earth Obs. Geoinf. 33, 119–126. http://dx.doi.org/10.1016/j.jag.2014.05.004.

Güneralp, İ., Rhoads, B.L., 2007. Continuous characterization of the planform geometry and curvature of meandering rivers. Geogr. Anal. 40, 1–25. http://dx.doi.org/10.1111/j.0016-7363.2007.00711.x.

Güneralp, İ., Rhoads, B.L., 2009. Empirical analysis of the planform curvature-migration relation of meandering rivers. Water Resour. Res. 45, W09424. http://dx.doi.org/10.1029/2008WR007533.

Güneralp, İ., Rhoads, B.L., 2010. Spatial autoregressive structure of meander evolution revisited. Geomorphology 120, 91–106. http://dx.doi.org/10.1016/j.geomorph.2010.02.010.

Güneralp, İ., Rhoads, B.L., 2011. Influence of floodplain erosional heterogeneity on planform complexity of meandering rivers. Geophys. Res. Lett. 38, 2–7. http://dx.doi.org/10.1029/2011GL048134.

Harmel, R., Haan, C., Dutnell, R., 1999. Evaluation of Rosgen's streambank erosion potential assessment in Northeast Oklahoma. J. Am. Water Resour. Assoc. 35, 113–121. http://dx.doi.org/10.1111/j.1752-1688.1999.tb05456.x.

Hooke, R., 1975. Distribution of sediment transport and shear stress in a meander bend. J. Geol. 83, 543–565.

Hubble, T.C.T., Docker, B.B., Rutherfurd, I.D., 2010. The role of riparian trees in maintaining riverbank stability: a review of Australian experience and practice. Ecol. Eng. 36, 292–304. http://dx.doi.org/10.1016/j.ecoleng.2009.04.006.

Hupp, C.R., Simon, A., 1991. Bank accretion and the development of vegetated depositional surfaces along modified alluvial channels. Geomorphology 4, 111–124. http://dx.doi.org/10.1016/0169-555X(91)90023-4.

Ikeda, S., Parker, G., Sawai, K., 1981. Bend theory of river meanders. Part 1. Linear development. J. Fluid Mech. 112, 363–377. http://dx.doi.org/10.1017/S0022112081000451.

Julian, J.P., Torres, R., 2006. Hydraulic erosion of cohesive riverbanks. Geomorphology 76, 193–206. http://dx.doi.org/10.1016/j.geomorph.2005.11.003.

Kemp, J., Olley, J., Ellison, T., McMahon, J., 2016. River response to European settlement in the subtropical Brisbane river, Australia. Anthropocene http://dx.doi.org/10.1016/j.ancene.2015.11.006.

Knox, J.C., 2006. Floodplain sedimentation in the upper Mississippi valley: natural versus human accelerated. Geomorphology 79, 286–310. http://dx.doi.org/10.1016/j.geomorph.2006.06.031.

Konsoer, K.M., Rhoads, B.L., Langendoen, E.J., Best, J.L., Ursic, M.E., Abad, J.D., Garcia, M.H., 2016. Spatial variability in bank resistance to erosion on a large meandering, mixed bedrock-alluvial river. Geomorphology 252, 80–97. http://dx.doi.org/10.1016/j.geomorph.2015.08.002.

Kronvang, B., Andersen, H.E., Larsen, S.E., Audet, J., 2013. Importance of bank erosion for sediment input, storage and export at the catchment scale. J. Soils Sediments 13, 230–241. http://dx.doi.org/10.1007/s11368-012-0597-7.

Kwan, H., Swanson, S., 2014. Prediction of annual streambank erosion for Sequoia National Forest, California. J. Am. Water Resour. Assoc. 50, 1439–1447. http://dx.doi.org/10.1111/jawr.12200.

Lawler, D.M., 1993. The measurement of river bank erosion and lateral channel change: a review. Earth Surf. Process. Landf. 18, 777–821. http://dx.doi.org/10.1002/esp.3290180905.

Lawler, D.M., Thorne, C.R., Hooke, J.M., 1997. Bank Erosion and Instability. In: Thorne, C.R., Hey, R.D., Newson, M.D. (Eds.), Applied Fluvial Geomorphology for River Engineering and Management. Wiley, Chichester, pp. 137–172.

Leopold, L.B., Wolman, M.G., 1960. River meanders. Geol. Soc. Am. Bull. 71, 769–793. http://dx.doi.org/10.1130/0016-7606(1960)71[769:RM]2.0.CO;2.

Lyons, N.J., Starek, M.J., Wegmann, K.W., Mitasova, H., 2015. Bank erosion of legacy sediment at the transition from vertical to lateral stream incision. Earth Surf. Process. Landf. 40, 1764–1778. http://dx.doi.org/10.1002/esp.3753.

Matsubara, Y., Howard, A.D., 2014. Modeling planform evolution of a mud-dominated meandering river: Quinn river, Nevada, USA. Earth Surf. Process. Landf. 39, 1365–1377. http://dx.doi.org/10.1002/esp.3588.

McMillan, M., 2016. Evaluating and Developing Streambank Erosion Models in the Gulf of Mexico oastal plain. The University of West Florida. Ph.D. Thesis.

Merritts, D.J., Walter, R.C., Rahnis, M., Hartranft, J., Cox, S., Gellis, A., Potter, N., Hilgartner, W., Langland, M., Manion, L., Lippincott, C., Siddiqui, S., Rehman, Z., Scheid, C., Kratz, L., Shilling, A., Jenschke, M., Datin, K., Cranmer, E., Reed, A., Matuszewski, D., Voli, M., Ohlson, E., Neugebauer, A., Ahamed, A., Neal, C., Winter, A., Becker, S., 2011. Anthropocene streams and base-level controls from historic dams in the unglaciated Mid-Atlantic Region, USA. Philos. Trans. R. Soc. A Math. Phys. Eng. Sci. 369, 976–1009. http://dx.doi.org/10.1098/rsta.2010.0335.

Metcalf, C.K., Wilkerson, S.D., Harman, W.A., 2009. Bankfull regional curves for North and Northwest Florida streams. J. Am. Water Resour. Assoc. 45, 1260–1272. http://dx.doi.org/10.1111/j.1752-1688.2009.00364.x.

Micheli, E.R., Kirchner, J.W., 2002. Effects of wet meadow riparian vegetation on streambank erosion. 2. Measurements of vegetated bank strength and consequences for failure mechanics. Earth Surf. Process. Landf. 27, 687–697. http://dx.doi.org/10.1002/esp.340.

Micheli, E.R., Kirchner, J.W., Larsen, E.W., 2004. Quantifying the effect of riparian forest versus agricultural vegetation on river meander migration rates, central Sacramento River, California, USA. River Res. Appl. 20, 537–548. http://dx.doi.org/10.1002/rra.756.

Mitchell, K.E., Lohmann, D., Houser, P.R., Wood, E.F., Schaake, J.C., Robock, A., Cosgrove, B. a., Sheffield, J., Duan, Q., Luo, L., Higgins, R.W., Pinker, R.T., Tarpley, J.D., Lettenmaier, D.P., Marshall, C.H., Entin, J.K., Pan, M., Shi, W., Koren, V., Meng, J., Ramsay, B.H., Bailey, A. a., 2004. The multi-institution North American land data assimilation system (NLDAS): utilizing multiple GCIP products and partners in a continental distributed hydrological modeling system. J. Geophys. Res. 109, http://dx.doi.org/10.1029/2003JD003823. D07S90.

Mosselman, E., 2014. Five common mistakes in fluvial morphodynamic modelling. Adv. Water Resour. 16, 6329. http://dx.doi.org/10.1016/j.advwatres.2015.07.025.

Odgaard, A.J., 1987. Streambank erosion along two rivers in Iowa. Water Resour. Res. 23, 1125–1236. http://dx.doi.org/10.1029/WR023i007p01225.

Odgaard, A.J., 1989. River-meander model. II: Applications. J. Hydraul. Eng. 115, 1451–1464. http://dx.doi.org/10.1061/(ASCE)0733-9429(1989)115:11(1451).

Osman, A.M., Thorne, C.R., 1988. Riverbank stability analysis. I: Theory. J. Hydraul. Eng. 114, 134–150. http://dx.doi.org/10.1061/(ASCE)0733-9429(1988)114:2(134).

Ottevanger, W., Blanckaert, K., Uijttewaal, W.S.J., 2012. Processes governing the flow redistribution in sharp river bends. Geomorphology 163-164, 45–55. http://dx.doi.org/10.1016/j.geomorph.2011.04.049.

Ottevanger, W., Blanckaert, K., Uijttewaal, W.S.J., de Vriend, H.J., 2013. Meander dynamics: a reduced-order nonlinear model without curvature restrictions for flow and bed morphology. J. Geophys. Res. Earth Surf. 118, 1118–1131. http://dx.doi.org/10.1002/jgrf.20080.

Parker, G., Shimizu, Y., Wilkerson, G.V., Eke, E.C., Abad, J.D., Lauer, J.W., Paola, C., Dietrich, W.E., Voller, V.R., 2011. A new framework for modeling the migration of meandering rivers. Earth Surf. Process. Landf. 36, 70–86. http://dx.doi.org/10.1002/esp.2113.

Partheniades, E., 1965. Erosion and deposition of cohesive soils. J. Hydraulics Div. Am. Soc. Civ. Eng. 91, 105–139.

Pelletier, J.D., 2012. A spatially distributed model for the long-term suspended sediment discharge and delivery ratio of drainage basins. J. Geophys. Res. 117, http://dx.doi.org/10.1029/2011JF002129. F02028.

Pelletier, J.D., Brad Murray, A., Pierce, J.L., Bierman, P.R., Breshears, D.D., Crosby, B.T., Ellis, M., Foufoula-Georgiou, E., Heimsath, A.M., Houser, C., Lancaster, N., Marani, M., Merritts, D.J., Moore, L.J., Pederson, J.L., Poulos, M.J., Rittenour, T.M., Rowland, J.C., Ruggiero, P., Ward, D.J., Wickert, A.D., Yager, E.M., 2015. Forecasting the response of Earth's surface to future climatic and land use changes: a review of methods and research needs. Earth's Future 3, 220–251. http://dx.doi.org/10.1002/2014EF000290.

Perucca, E., Camporeale, C., Ridolfi, L., 2007. Significance of the riparian vegetation dynamics on meandering river morphodynamics. Water Resour. Res. 43, http://dx.doi.org/10.1029/2006WR005234. W03430.

Pizzuto, J.E., 1984. Bank erodibility of shallow sandbed streams. Earth Surf. Process. Landf. 9, 113–124. http://dx.doi.org/10.1002/esp.3290090203.

Pizzuto, J.E., Meckelnburg, T.S., 1989. Evaluation of a linear bank erosion equation. Water Resour. Res. 25, 1005–1013. http://dx.doi.org/10.1029/WR025i005p01005.

Pizzuto, J.E., O'Neal, M., 2009. Increased mid-twentieth century riverbank erosion rates related to the demise of Mill Dams, South River, Virginia. Geology 37, 19–22. http://dx.doi.org/10.1130/G25207A.1.

Pizzuto, J.E., O'Neal, M., Stotts, S., 2010. On the retreat of forested, cohesive riverbanks. Geomorphology 116, 341–352. http://dx.doi.org/10.1016/j.geomorph.2009.11.008.

Pollen, N., 2007. Temporal and spatial variability in root reinforcement of streambanks: accounting for soil shear strength and moisture. Catena 69, 197–205. http://dx.doi.org/10.1016/j.catena.2006.05.004.

Pollen, N., Simon, A., 2005. Estimating the mechanical effects of riparian vegetation on stream bank stability using a fiber bundle model. Water Resour. Res. 41, W07025. http://dx.doi.org/10.1029/2004WR003801.

Rosgen, D.L., 1994. A classification of natural rivers. Catena 22, 169–199. http://dx.doi.org/10.1016/0341-8162(94)90001-9.

Please cite this article as: M. McMillan, Z. Hu, A watershed scale spatially-distributed model for streambank erosion rate driven by channel curvature, Geomorphology (2016), http://dx.doi.org/10.1016/j.geomorph.2017.03.017

Rosgen, D.L., 2001. A Practical Method of Computing Streambank Erosion Rate. Proceedings of the Seventh Federal Interagency Sedimentation Conference. US Inter-agency Committee on Water Resources, Subcommittee on Sedimentation., pp. 9–18.
Rosgen, D.L., 2009. Watershed Assessment of River Stability and Sediment Supply. 2nd ed., Wildland Hydrology.
Rossi, M.W., Whipple, K.X., Vivoni, E.R., 2016. Precipitation and evapotranspiration controls on daily runoff variability in the contiguous United States and Puerto Rico. J. Geophys. Res. Earth Surf. 121, 128–145. http://dx.doi.org/10.1002/2015JF003446.
Sass, C.K., Keane, T.D., 2012. Application of Rosgen's BANCS model for NE Kansas and the development of predictive streambank erosion curves. J. Am. Water Resour. Assoc. 48, 774–787. http://dx.doi.org/10.1111/j.1752-1688.2012.00644.x.
Sefick, S.A., Kalin, L., Kosnicki, E., Schneid, B.P., Jarrell, M.S., Anderson, C.J., Paller, M.H., Feminella, J.W., 2015. Empirical estimation of stream discharge using channel geometry in low-gradient, sand-bed streams of the Southeastern Plains. J. Am. Water Resour. Assoc. 51, 1060–1071. http://dx.doi.org/10.1111/jawr.12278.
Sekely, A., Mulla, D., Bauer, D., 2002. Streambank slumping and its contribution to the phosphorus and suspended sediment loads of the Blue Earth River, Minnesota. J. Soil Water Conserv. 57, 243–250.
Sexton, J.O., Song, X.-P., Feng, M., Noojipady, P., Anand, A., Huang, C., Kim, D.-H., Collins, K.M., Channan, S., Dimiceli, C., Townshend, J.R., 2013. Global, 30-m resolution continuous fields of tree cover: Landsat-based rescaling of MODIS vegetation continuous fields with lidar-based estimates of error. Int. J. Digital Earth 6, 427–448. http://dx.doi.org/10.1080/17538947.2013.786146.
Simon, A., Curini, A., Darby, S., Langendoen, E., 2000. Bank and near-bank processes in an incised channel. Geomorphology 35, 193–217. http://dx.doi.org/10.1016/S0169-555X(00)00036-2.
Simon, A., Doyle, M., 2007. Critical evaluation of how the Rosgen classification and associated "Natural Channel Design" methods fail to integrate and quantify fluvial processes and channel response. J. Am. Water Resour. Assoc. 43, 1117–1131.
Stott, T., 1997. A comparison of stream bank erosion processes on forested and moorland streams in the Balquhidder Catchments, central Scotland. Earth Surf. Process. Landf. 22, 383–399. http://dx.doi.org/10.1002/(SICI)1096-9837(199704)22:4¡383::AID-ESP695¿3.0.CO;2-4.
Thomas, R.E., Pollen-Bankhead, N., 2010. Modeling root-reinforcement with a fiber-bundle model and Monte Carlo simulation. Ecol. Eng. 36, 47–61. http://dx.doi.org/10.1016/j.ecoleng.2009.09.008.
Thorne, C., 1982. Processes and Mechanisms of River Bank Erosion. In: Hey, R., Bathurst, J., Thorne, C. (Eds.), Gravel-Bed Rivers: Processes, Tools, Environments. Wiley, Chichester, pp. 227–271.
Thorne, S.D., Furbish, D.J., 1995. Influences of coarse bank roughness on flow within a sharply curved river bend. Geomorphology 12, 241–257. http://dx.doi.org/10.1016/0169-555X(95)00007-R.
Tiwari, H., Das, P., Bharti, A.K., 2012. MATLAB Programming solution for critical and normal depth in trapezoidal channels. Int. J. Eng. Res. Tech. 1, 1–3.
Environmental Protection Agency, U.S., 2000. National Water Quality Inventory.
Van Eps, M.A., Formica, S.J., Morris, T.L., Beck, J.M., Cotter, A.S., 2004. Using a Bank Erosion Hazard Index (BEHI) to Estimate Annual Sediment Loads from Streambank Erosion in the West Fork White River Watershed. Self-sustaining Solutions for Streams, Wetlands, and Watersheds, 12–15, September 2004, American Society of Agricultural and Biological Engineers. American Society of Agricultural and Biological Engineers., http://dx.doi.org/10.13031/2013.17386.
Vatankhah, A.R., 2013. Explicit solutions for critical and normal depths in trapezoidal and parabolic open channels. Ain Shams Eng. J. 4, 17–23. http://dx.doi.org/10.1016/j.asej.2012.05.002.
de Vente, J., Poesen, J., Verstraeten, G., Govers, G., Vanmaercke, M., Van Rompaey, A., Arabkhedri, M., Boix-Fayos, C., 2013. Predicting soil erosion and sediment yield at regional scales: where do we stand? Earth Sci. Rev. 127, 16–29. http://dx.doi.org/10.1016/j.earscirev.2013.08.014.
Walter, R.C., Merritts, D.J., 2008. Natural streams and the legacy of water-powered mills. Science 319, 299–304. http://dx.doi.org/10.1126/science.1151716.
Wilkinson, S.N., Dougall, C., Kinsey-Henderson, A.E., Searle, R.D., Ellis, R.J., Bartley, R., 2014. Development of a time-stepping sediment budget model for assessing land use impacts in large river basins. Sci. Total. Environ. 468-469, 1210–1224. http://dx.doi.org/10.1016/j.scitotenv.2013.07.049.
Wilkinson, S.N., Prosser, I.P., Rustomji, P., Read, A.M., 2009. Modelling and testing spatially distributed sediment budgets to relate erosion processes to sediment yields. Environ. Model. Softw. 24, 489–501. http://dx.doi.org/10.1016/j.envsoft.2008.09.006.
Wynn, T.M., Mostaghimi, S., 2006. The effects of vegetation and soil type on streambank erosion, Southwestern Virginia, USA. J. Am. Water Resour. Assoc. 42, 69–82. http://dx.doi.org/10.1111/j.1752-1688.2006.tb03824.x.
Xia, Y., Mitchell, K., Ek, M., Cosgrove, B., Sheffield, J., Luo, L., Alonge, C., Wei, H., Meng, J., Livneh, B., Duan, Q., Lohmann, D., 2012. Continental-scale water and energy flux analysis and validation for North American land data assimilation system project phase 2 (NLDAS-2): 2. Validation of model-simulated streamflow. J. Geophys. Res.: Atmos. 117, http://dx.doi.org/10.1029/2011JD016051. D03110.
Xiao, X., White, E.P., Hooten, M.B., Durham, S.L., 2011. On the use of log-transformation vs. nonlinear regression for analyzing biological power laws. Ecology 92, 1887–1894. http://dx.doi.org/10.1890/11-0538.1.
Zeng, X., 2001. Global vegetation root distribution for land modeling. J. Hydrometeorol. 2, 525–530. http://dx.doi.org/10.1175/1525-7541(2001)002¡0525:GVRDFL¿2.0.CO;2.

Please cite this article as: M. McMillan, Z. Hu, A watershed scale spatially-distributed model for streambank erosion rate driven by channel curvature, Geomorphology (2016), http://dx.doi.org/10.1016/j.geomorph.2017.03.017